CANADIAN THESES

THÈSES CANADIENNES

NOTICE

The quality of this microfiche is heavily dependent upon the quality of the original thesis submitted for microfilming. Every effort has been made to ensure the highest quality of reproduction possible.

If pages are missing, contact the university which granted the degree.

Some pages may have indistinct print especially if the original pages were typed with a poor typewriter ribbon or if the university sent us an inferior photocopy.

Previously copyrighted materials (journal articles, published tests, etc.) are not filmed.

Reproduction in full or in part of this film is governed by the Canadian Copyright Act, R.S.C. 1970, c. C-30. Please read the authorization forms which accompany this thesis.

AVIS

La qualité de cette microfiche dépend grandement de la qualité de la thèse soumise au microfilmage. Nous avons tout fait pour assurer une qualité supérieure de reproduction.

S'il manque des pages, veuillez communiquer avec l'université qui a conféré le grade.

La qualité d'impression de certaines pages peut laisser à désirer, surtout si les pages originales ont été dactylographiées à l'aide d'un ruban usé ou si l'université nous a fait parvenir une photocopie de qualité inférieure.

Les documents qui font déjà l'objet d'un droit d'auteur (articles de revue, examens publiés, etc.) ne sont pas microfilmés.

La reproduction, même partielle, de ce microfilm est soumise à la Loi canadienne sur le droit d'auteur, SRC 1970, c. C-30. Veuillez prendre connaissance des formules d'autorisation qui accompagnent cette thèse.

THIS DISSERTATION
HAS BEEN MICROFILMED
EXACTLY AS RECEIVED

LA THÈSE A ÉTÉ
MICROFILMÉE TELLE QUE
NOUS L'AVONS REÇUE

184

0-315-26916-2

National Library of Canada | Bibliothèque nationale du Canada

Canadian Theses Division | Division des thèses canadiennes

Ottawa, Canada
K1A 0N4

PERMISSION TO MICROFILM — AUTORISATION DE MICROFILMER

• Please print or type — Écrire en lettres moulées ou dactylographier

Full Name of Author — Nom complet de l'auteur

Rogelio Muñoz

Date of Birth — Date de naissance	Country of Birth — Lieu de naissance
August 12, 1953	México

Permanent Address — Résidence fixe

Luis Moya # 220
Morelia, Mich. 5800
México

Title of Thesis — Titre de la thèse

Inelastic Cross-sections for fast-electron Collisions

University — Université

University of Alberta

Degree for which thesis was presented — Grade pour lequel cette thèse fut présentée

M. Sc.

Year this degree conferred — Année d'obtention de ce grade	Name of Supervisor — Nom du directeur de thèse
1983	Dr. R. F. Egerton

Permission is hereby granted to the NATIONAL LIBRARY OF CANADA to microfilm this thesis and to lend or sell copies of the film.

The author reserves other publication rights, and neither the thesis nor extensive extracts from it may be printed or otherwise reproduced without the author's written permission.

L'autorisation est, par la présente, accordée à la BIBLIOTHÈQUE NATIONALE DU CANADA de microfilmer cette thèse et de prêter ou de vendre des exemplaires du film.

L'auteur se réserve les autres droits de publication; ni la thèse ni de longs extraits de celle-ci ne doivent être imprimés ou autrement reproduits sans l'autorisation écrite de l'auteur.

Date	Signature
August 5, 1983	

NL-91 (4/77)

THE UNIVERSITY OF ALBERTA

INELASTIC CROSS-SECTIONS FOR FAST-ELECTRON COLLISIONS

by

© ROGELIO MUNOZ

A THESIS

SUBMITTED TO THE FACULTY OF GRADUATE STUDIES AND RESEARCH

IN PARTIAL FULFILMENT OF THE REQUIREMENTS FOR THE DEGREE

OF MASTER OF SCIENCE

DEPARTMENT OF PHYSICS

EDMONTON, ALBERTA

FALL 1983

THE UNIVERSITY OF ALBERTA

RELEASE FORM

NAME OF AUTHOR ROGELIO MUNOZ

TITLE OF THESIS INELASTIC CROSS-SECTIONS FOR FAST-ELECTRON COLLISIONS

DEGREE FOR WHICH THESIS WAS PRESENTED MASTER OF SCIENCE

YEAR THIS DEGREE GRANTED FALL 1983

(SIGNED) .....

PERMANENT ADDRESS:

Luis Moya #220

Morelia, Michoacan 5800

MEXICO

DATED August 3 1983

THE UNIVERSITY OF ALBERTA

FACULTY OF GRADUATE STUDIES AND RESEARCH

The undersigned certify that they have read, and recommend to the Faculty of Graduate Studies and Research, for acceptance, a thesis entitled **INELASTIC CROSS-SECTIONS FOR FAST-ELECTRON COLLISIONS** submitted by ROGELIO MUNOZ in partial fulfilment of the requirements for the degree of MASTER OF SCIENCE.

R. F. Egerton
.....
Supervisor

.....

.....

.....

Date...July 28, 1983.....

In the memory of my beloved father

ABSTRACT

Transmission electron energy-loss has been used to determine the angular and energy dependence of the cross-section for K-shell ionization of Al, and L-shell ionization of Cr, Fe, and Cu. On the basis of these experimental results it was found that simple hydrogenic theory predicts well the angular distribution of inner-shell scattering and shows a reasonable absolute agreement for a large energy window. In addition, total-inelastic cross-sections for these elements were measured and compared with Lenz, Hartree-Slater, and Plasmon theory. The experiments show that a free-electron plasmon model predicts fairly well the cross-section for elements such as Al. For Cr, Fe, and Cu an atomic model is more appropriate.

A C K N O W L E D G E M E N T S

I would like to thank Dr. R.F. Egerton for his excellent supervision and many stimulating discussions on EELS. I am also greatful to the members of my supervisory committee.

I would also like to thank the Mexican Council of Science and Technology for a scholarship and the Department of Physics for a partial Graduate Assistantship.

Finally, I would like to thank my wife Lulú, my daughter Sandra, and my son Alejandro, who have actively encouraged and supported my efforts in every way.

Table of Contents

List of Figures

CHAPTER I

BASIC PRINCIPLES OF EELS AND INTRODUCTION TO THE PRESENT STUDY

1.1 INTRODUCTION

With the first papers dealing with collisions of fast particles with atoms, which appeared at the beginning of this century, there began a new technique for studying the structure of matter by means of this process. The process generally represents the interaction of particles (in this case electrons) with atoms, the latter sometimes called the target and the phenomenon itself scattering. Thus, a scattering process depends on the characteristics of the incident electrons and the atomic properties of the target (here we use the words specimen and sample as synohymous with target). The characteristics of the incident electrons depend on how fast they are approaching the scattering atom, i.e. on the wave vector $\vec{k}$, while the atomic properties are generally described by probabilities of transition; these probabilities are related to the kind of atomic wave function assumed and consequently to the atomic potential. When the incident electrons interact with the atomic potential, the former may be deviated from their original direction (scattered). There are basically two types of scattering process: elastic and inelastic. In the former, the incident particles transfer momentum, and in the latter transfer momentum and appreciable energy to the atoms of the

sample. This latter mechanism by which fast electrons (with kinetic energy greater than about 10keV) interact with a sample is the main concern in the present thesis.

If a beam of fast electrons impinges upon a sample, and the sample is thin enough so that most of the beam is not absorbed, it is convenient to classify the transmitted electrons into three categories: (1) the unscattered beam, (2) the elastically scattered beam, and (3) the inelastically scattered beam. These groups are characterized primarily on the basis of scattering mechanism and how much energy has been lost by the electrons in passing through the material. The third group of electrons that are transmitted through a thin sample are those that have interacted with the electrons within the sample and lost energy in the process. The amount of energy lost depends largely on the material being studied. That is, the distribution of energy losses is material dependent and it is this property that we are going to use for obtaining information about the atomic properties of the sample. The utilization of the transmitted energy loss distribution to determine chemical and structural properties of a thin sample is known as Electron Energy-Loss Spectroscopy (EELS).

1.2 BASIC PRINCIPLES OF EELS

When electrons impinge upon a sample, a variety of processes occur. The electron may interact with the atomic nuclei, with the inner orbital electrons (having discrete

energy levels), or with electrons in the outer shells (possesing a range of energies). All of these processes result in a change in the energy of the incident electrons which can be measured to give information concerning the nature of the target material. When the incident electrons interact with the inner-shell electrons or with the relatively free outer-shell electrons, they may excite these atomic electrons to higher energy levels or eject them completely from the atom (ionization). In causing excitation or ionization, the incident electrons themselves lose energy. Low energy losses are associated with excitation of plasmons or valence-electron transitions while higher energy losses are due to the excitation or ionization of inner orbital electrons and are characteristic of the element being ionized. It is these higher energy losses which are measured for the purpose of elemental analysis (Isaacson and Johnson 1975, Colliex *et al.* 1976, and Egerton 1979b). Typical electron losses incurred during these ionization processes are in the range 50-2000eV for light elements.

1.3 INTRODUCTION TO THE PRESENT STUDY

Cross-sections for inelastic scattering of fast electrons by atoms are of concern in many branches of Physics. One such area is electron microscopy, in particular EELS where a partial cross-section $\sigma_k(\alpha,\Delta)$ for ionization of shell k (=K, L, M, etc.) by fast incident electrons [which are thereby scattered through angles $<\alpha$ and suffer energy

losses between E_k and $E_k+\Delta$, E_k being the ionization energy of shell k] is required for quantitative microanalysis of light elements (Joy *et al.* 1979). Also total inelastic cross-sections σ_{in} (i.e., the sum of all possible inelastic collison cross-sections) are required for estimating the local thickness of a specimen (Hosoi *et al.* 1981). Both $\sigma_k(\alpha,\Delta)$ and σ_{in} can be measured experimentally using a thin sample of known thickness and composition or may be calculated on the basis of an atomic model (Chapter II). Since these calculations neglect certain factors (such as solid state effects), it is of interest to compare the theoretical results with experimental data. In this thesis, we present such a comparison for Aluminum, Chromium, Iron, and Copper (Chapter IV).

CHAPTER II

CALCULATIONS OF INELASTIC CROSS-SECTIONS

2.1 INTRODUCTION

Inelastic cross-sections specify the probability of an incident electron being inelastically scattered by an atomic electron of a sample. The probability of an atomic electron being excited to a certain energy is given by the Generalized Oscillator Strength (GOS). The GOS is proportional to the differential cross-section, which is the main concern in this Chapter. Here, we are going to present the different alternatives for calculating inelastic cross-sections which may be prominent in EELS. In an inelastic process, the incident electrons lose energy in the interaction with matter. This energy loss is attributable to excitation of atomic electrons, both inner-shell electrons and outer-shell electrons. The probability for any of these excitations to occur is given by the corresponding cross-section. In the following sections we present: First, the general considerations for calculating inelastic cross-sections; second, the different atomic models used to calculate inner-shell ionization cross-sections; and finally, we present the different models used to calculate total-inelastic cross-sections (i.e. the sum of all possible inelastic-collision cross-sections).

2.2 GENERAL CONSIDERATIONS

In calculating cross-sections, there are three procedures of different degrees of refinement, these are:

Hartree-Fock-Slater Approximation (Hartree 1928, Fock 1930, and Slater 1930). This approximation consists of describing the many-particle problem by an independent particle model in which each electron in turn is considered exposed to the field of the nucleus and the average field of the remaining electrons. Fock included the fact that the incoming electron can exchange roles with one of the atomic electrons (exchange). Finally, Slater modified the mathematical method involved (variational treatment).

Thomas-Fermi Model. While in the Hartree method the individual electron still exists, it disappears in the statistical approach due to Thomas (1926) and Fermi (1928). The many-electron atom is considered as a nucleus surrounded by an electron gas which forms a spherical atmosphere of variable density. The limitations of this model are inherent in the statistical treatment of the electrons, which makes the approach fairly adequate only for atoms with a high number of electrons ($Z>40$). There is a modification of the Thomas-Fermi method by Dirac (1930), which takes exchange of the electrons into account.

Mathematical Approximations. These approximations are based on analytical expressions for the atomic potential and/or analytical expressions for the atomic wave functions.

The methods described previously have been used to calculate both elastic and inelastic cross-sections, since both calculations necessarly involve the assumption of an atomic potential to calculate the atomic wave functions. These wave functions may also have an analytical form for a given atomic potential.

A method similar to that used to calculate elastic cross-sections can be used to calculate cross-sections for inelastic collisions of fast electrons with atoms. Hence, the inelastic scattering may be treated by regarding the atom as a static center of force which gives to an electron a potential energy V(r). This potential is usually taken as spherically symmetrical. Furthermore, for sufficiently fast collisions, the influence of the incident electron upon an atom may be regarded as a sudden and weak perturbation; that is, the first Born approximation can be used. According to Born's theory (Born 1926), when a plane wave strikes the atom each volume element in the atom sends out a spherical wavelet. These wavelets start in phase but possess different amplitudes depending upon the value of the potential at the volume element. In the first Born approximation, both the incident and scattered electrons are treated as plane waves.

The first step towards obtaining inelastic cross-sections is to calculate the probability of transition from an initial (ground) to a final (excited) state; that is, to calculate GOS (Generalized Oscillator Strength). Ideally this would be done by solving the Schrodinger

scattering) for the complete system, i.e., the wave equation which contains explicity the coordinates of both the incident and atomic electrons. The energy term is the sum of the energy of the atom in its ground state and the kinetic energy of the incident electron. The solutions of this equation are generally assumed to be separable into a function of the incident electron and another function for the atom.

The energy differential cross-section for a collision, in which an incident electron of kinetic energy T is scattered with a momentum change $\hbar\vec{K}=\hbar(\vec{k}-\vec{k}')$ and energy loss E, is given in the first Born approximation by (Bethe 1930, Inokuti 1971)

$$\frac{d\sigma_n}{dE} = \int_{K_{min}}^{K_{max}} \frac{4\pi a_o}{(T/R)\ (E/R)} \frac{df_n(E,K)}{dE}\ d[\ln(Ka_o)^2] \qquad (2.1)$$

where a_o is the Bohr radius; $R=me^4/2\hbar^2=13.6eV$ is the Rydberg energy. An important point about eq. (2.1), discovered by Bethe (1930), is that the GOS, $df_n(E,K)/dE$, should be independent of T if T is sufficiently large. In such a case, the GOS can be computed from internal dynamics of the atom by means of the following relation (Inokuti 1971):

$$\frac{df_n(E,K)}{dE} = (E/R)(Ka_o)^{-2} \left|\int u_n^*(r_1,..,r_z)\sum_{j=1}^{z}\exp(i\vec{K}\cdot\vec{r})u_o(r_1,..,r_z)dr_1,..,dr_z\right|^2 \qquad (2.2)$$

with r_j being the position vector of the jth atomic electron, $u_0(r_1,..,r_z)$ and $u_n(r_1,..,r_z)$ the wave functions of the atomic electrons in the initial and final state. The total wave functions of the initial and final state are

$\psi_o = u_o \exp(i\vec{k}\cdot\vec{r}_j)$ and $\psi_n = u_n \exp(i\vec{k}'\cdot\vec{r}_j)$, respectively. These, of course, should satisfy the Schrodinger equation. We may rewrite eq. (2.2) in a more convenient form given by

$$\frac{df_{n1}(E,K)}{dE} = \frac{2m_o E}{\hbar^2 K^2} \sum_{l'} |\langle \epsilon l' | \exp(i\vec{K}\cdot\vec{r}) | n l \rangle|^2 \qquad (2.3)$$

where $\langle n| \; |0\rangle$ denotes an atomic matrix element between the excited state n and the ground state. This matrix element depends on the quantum numbers involved in the transition. For a single atom the possible transitions are between occupied and unoccupied single-electron states of the atom, transitions to occupied states being forbidden by the Pauli exclusion principle.

It should be pointed out that eq. (2.1) was derived assuming a Coulombic interaction, i.e., the potential V(r) may be written as

$$V(r) = \frac{Ze^2}{r} - \sum_{j=1}^{z} \frac{e^2}{|\vec{r}-\vec{r}_j|} \qquad (2.4)$$

Here the first term is the potential energy of the electron in the field of the nucleus of charge Ze. The second term is the potential of interaction due to the fast electron at position r and an atomic electron labeled r_j.

Since exact atomic wave functions for the initial and final states, u_o and u_n, are seldom available, approximate methods have been developed to calculate these wave functions. These methods have given rise to different methods for the computation of GOS by means of eq. (2.2) and consequently for the computation of inelastic cross-sections

by means of eq. (2.1). Some of thse methods are described in the following sections.

2.3 INNER-SHELL IONIZATION CROSS-SECTIONS

By an inner-shell ionization cross-section, one means the cross-section for excitation of electrons from an inner shell of an atom to the continuum. Different approaches have been developed to carry out these calculations; some of them are based on simple hydrogenic wave functions and others are based on more sophisticated computational methods to obtain more accurate atomic wave functions. Among these methods we describe those which may be relevant to EELS.

2.3.1 THE HYDROGENIC MODEL

Egerton (1979a) has proposed the use of a simple hydrogenic model to compute partial or total K- and L-shell cross-sections needed to carry out elemental analysis by means of EELS. The model is based on previous hydrogenic approximations (Bethe 1930, Inokuti 1971) which use Coulombic-type wave functions.

An important point about Coulombic-type wave functions is the choice of a screening parameter. Because the choice is crucial to all calculations involving such wave functions, we shall make some comments about the screening parameter.

The basic assumption underlying the use of screened hydrogen-like wave functions to describe a many-electron

atom is that for a single electron outside a closed shell, the field due to the nucleus and the other electrons taken together can be assumed to be spherically symmetrical, that is, to behave as 1/r. Once this assumption is made, the effect of the other electrons is accomodated by replacing the nuclear charge Z by an approximate effective charge $Z_s = Z - \Delta Z$, ΔZ being a number characteristic of the n and l values of the electrons in the shell. The actual choice of ΔZ would depend on what criterion one uses to compare a physical many-electron atom with its idealized hydrogenic counterpart. In other words, different atomic properties are differently affected by the presence of the other electrons and one has to decide what property one would use to define ΔZ, assuming that the total effect on this property can be represented by an apparent decrease in the nuclear charge. Having decided on this parameter, one makes another vital assumption: that for a given n and l, the normalized radial wave functions for atoms of different atomic number Z are similar ; i.e., they are replicas of the same function on different scales (scaled wave functions).

Assumptions of the hydrogenic model. In addition to the considerations made in section 2.2, the hydrogenic calculations are based on the following assumptions:

(1) Relativistic effects within the atom (due to the high orbital velocity of atomic electrons, on a classical picture) are neglected. Relativistic effects due to the high velocity v_0 of the incident electron can be incorporated to

first order by avoiding the approximation: $E_0 = (1/2)mv^2$; instead the incident electron may be characterized by the parameter $T[=(1/2)m_0v^2$, m_0=electron rest mass].

(2) In common with other calculations of inner-shell cross-sections, an atomic model is assumed. That is, solid state effects are ignored; the cross-section for a given atom (integrated over an energy range greater than 50 eV) is assumed to be independent of its physical and chemical environment.

(3) Exchange effects (which are possible because the incident and atomic electrons are the same type of particle and can interchange roles) are neglected.

(4) The wave functions used for the initial and final state of *1s* electrons are solutions of the Schrodinger equation for the hydrogen atom, scaled to take into account the effective potential of the nucleus.

(5) The screening effect of outer shells is accounted for (to first order) by adding to the nuclear potential energy a term E_s, corresponding to an approximately spherical distribution of outer charge. Screening of the nuclear field by the second K-electron is included by using an effective nuclear charge of $Z_s=Z-\Delta Z$, ΔZ taken as the value 0.3125 calculated by Zener (1930).

(6) For L-shell ionization, the hydrogenic model in its basic form predicts too large a cross-section at an energy near the ionization edge; the calculations must be modified by adding an energy dependence to the GOS, to bring this

into agreement with X-ray absorption measurements, for example (Egerton 1981).

The generalized oscillator strength. The first step towards obtaining cross-sections is to calculate the GOS for a transition which absorbs energy E and momentum hK from the incident electron. In the hydrogenic model, the initial and final state, u_o and u_n in eq. (2.2), are scaled Coulombic wave functions which yield an analytical form for the GOS which can be evaluated and integrated over scattering angle and energy loss by means of a short (<100 line) computer program (Egerton 1979). The GOS, as indicated in the section 2.1, is a fundamental property of the atom and the full momentum-transfer dependence of the ionization cross-section is implicity contained in it. The GOS for a given atom can be represented comprehensively by a 3-dimensional plot of $df_n(E,K)/dE$ as a function of $\ln(Ka_o)^2$ and E. A surface resulting from that plot is called the Bethe surface (Inokuti 1971). As an example, the hydrogenic GOS for carbon K-shell excitation is shown as a function of E and $\ln(Ka_o)^2$ in figure 2.1. In this figure two main features can be observed: First, individual curves show qualitatively the angular dependence of K-shell scattering, for different amounts of energy loss. For an energy loss not much larger than the threshold value E_k, the scattering is forward-peaked (i.e. is of maximum intensity at θ=0) whereas for large energy loss (several times E_k) the scattered electrons are concentrated around an angle given by

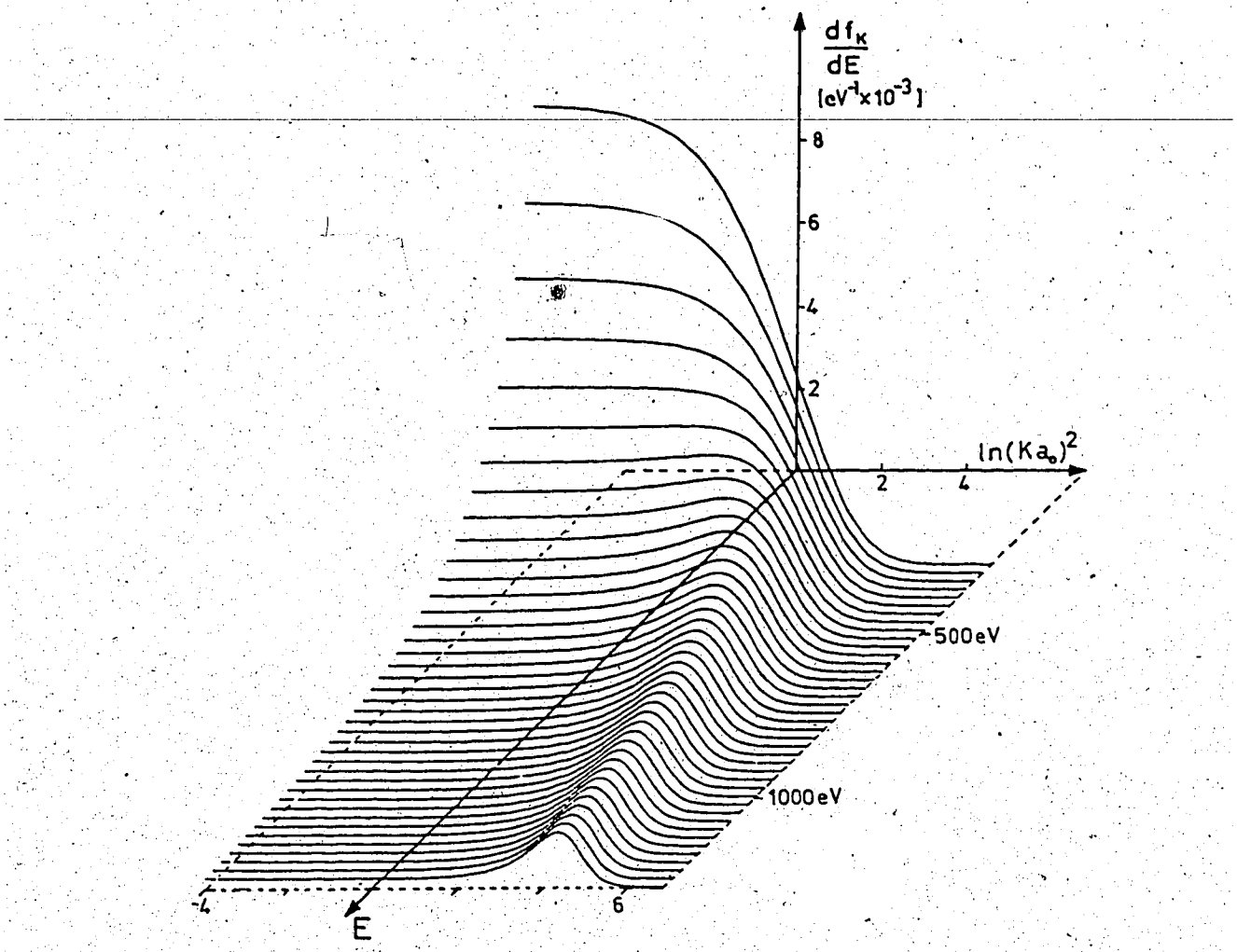

Figure 2.1 The Bethe surface for K-shell ionization in carbon, calculated from the hydrogenic model (Egerton 1979a).

$(Ka_o)^2=E/R$, forming a Bethe ridge which represents hard collisions, that is, those with small impact parameter. Second, the energy dependence of GOS is represented by cross-sections through the Bethe surface at constant K: in particular, planes corresponding to very small K give the optical oscillator strength, which is proportional to the photoabsorption cross-section.

The energy differential cross-section. The number of incident electrons scattered as a result of K-shell excitation into angles less than α and energy loss E can be obtained by integration of eq. (2.1) over appropriate limits of integration: $(Ka_o)^2_{min}$ and $(Ka_o)^2_{max}$, which may be obtained from the scattering kinematics (conservation of momentum and energy). The energy-differential cross-section, $d\sigma_k(\alpha)/dE$, computed from the hydrogenic model for various values of α and E shows (see fig. 2.2) an approximate energy dependence of the form

$$\frac{d\sigma_K}{dE} \propto E^{-s} \qquad (2.5)$$

Partial cross-sections. The partial cross-sections $\sigma_k(\alpha,\Delta)$, which specify the probability of K-shell scattering through angles up to α and with energy losses covering a range Δ above E_k (the binding energy), is given by

$$\sigma_K(\alpha,\Delta)= \int_{E_K}^{E_K+\Delta} \frac{d\sigma_K(\alpha)}{dE}\, dE \qquad (2.6)$$

For numerical integration of this equation, use was made of the approximate power-law dependence, eq. (2.5), to reduce

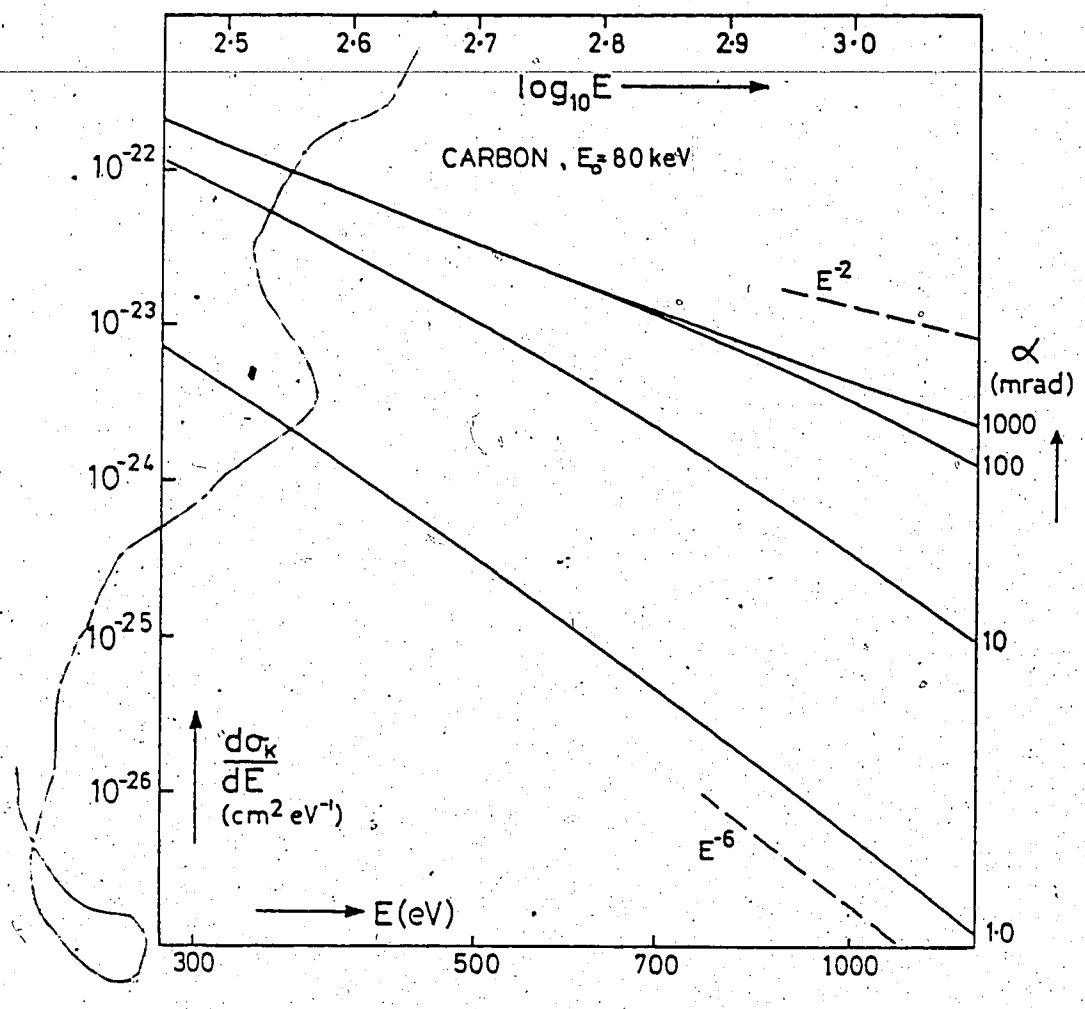

Figure 2.2 The K-shell energy-loss spectrum of carbon for 80 keV incident electrons and various collection semi-angle α (Egerton 1979).

the number of steps required, S being calculated for each energy increment. In Chapter IV we present some hydrogenic calculations for selected elements for comparison with experimental results.

Integral and Total cross-sections. For large Δ, the partial cross section $\sigma_k(\alpha,\Delta)$ becomes equal to the integral cross-section $\sigma_k(\alpha)$ for K-shell scattering into angles up to α and any energy loss above the threshold E_k. $\sigma_k(\alpha)$ can be evaluated numerically as:

$$\sigma_K(\alpha) = \int_{E_K}^{E_2} \frac{d\sigma_K(\alpha)}{dE} \, dE \qquad (2.7)$$

where E_2 is chosen such that contributions to the integral from higher energy losses can be neglected. In the limiting case $\alpha=\pi$, eq. (2.7) gives the total cross-section for K-shell scattering. Again, to calculate L-shell cross-sections, a modified hydrogenic model can be used.

2.3.2 HARTREE-SLATER MODEL

A nonrelativistic Hartree-Slater central-field model was used by Leapman, Rez, and Mayers (1980) to calculate cross-sections for ionization of atomic K-, L-, and M-shells by fast electrons. The *Hartree-Slater* (HS) terminology was first used by Manson (1972) to indicate the use of Hartree wave functions with the Slater approximation for exchange. Manson also pointed out that the more usual *Hartree-Fock-Slater* terminology incorrectly suggests an improvement on the Fock exchange.

In the central field approximation, the radial part of the single-particle orbital satisfies the Schrödinger equation

$$\frac{\hbar^2}{2m}\frac{d^2R_{nl}}{dr^2} + [\varepsilon - V(r) - \frac{l(l+1)}{2mr^2}]R_{nl} = 0 \qquad (2.8)$$

Here ϵ is the single-particle energy eigenvalue. An interesting point about this equation is that the potential $V(r)$ seen by an electron in the orbital (nl) depends on the orbital. To solve this equation, Hartree (1928) suggested the following procedure. By associating a charge density $\rho(r) = -4\pi e R_{n,l}^2(r)$ with each electron, we could construct a tentative potential from the total charge distribution due to the electrons and the nucleus. Solving eq. (2.8), we could obtain solutions $R_{n,l}(r)$ which now determine a new potential. This procedure is continued until the final wave function is self-consistent to a high order of accurancy.

Assumptions of the Hartree-Slater Model. The calculations carried out by Leapman, Rez and Mayers (1980) are based on previous calculation done by Manson (1972) and McGuire (1971) who make use of the general considerations mentioned in section 2.2. In addition, the following assuptions are made:

(1) Relativistic effects within the atom are neglected. Relativistic effects due to the high velocity v of the incident electron are accounted by using $E_0 = (1/2)m_0v^2$ instead of the most general expression $E = mc^2 - m_0c^2$

(2) An atomic model is assumed. Consequently, solid state effects are neglected.

(3) Exchange between the scattered electron and the ejected atomic electron is not taken into account, since this effect is negligible except for very high energy losses and scattering angles.

(4) The initial and final states of the atom are expressed as products of one-electron wave functions for a central atomic potential. Thus, wave functions of the electrons not directly involved in the transition remain unaltered.

(5) The initial state is a one-electron Herman-Skillman wave function, a solution of the Schrödinger equation with the self-consistent atomic potential:

$$V_{1s}^{self}(r)=(2/r)[1-(1+Z_o r)\exp(-2Z_o/r)] \qquad (2.9)$$

where Z_o is the effective screened nuclear charge for a *1s* electron. The final states are found by solving the radial Schrödinger equation, eq. (2.8), with the same central field for the continuum energies. The outer states are normalized by matching Coulomb wave functions at large radius.

The generalized oscillator strength. The GOS needed to calculate the cross-sections is calculated by computing the matrix elements in the following equation [*cf.* eq. (2.3)]

$$\frac{df_{nl}(E,K)}{dE} = \frac{2m_o E}{\hbar^2 K^2} \sum_{l'} |\langle \varepsilon l' | \exp(i\vec{K}\cdot\vec{r}) | nl \rangle|^2 \qquad (2.10)$$

Here, *n* and *l* refer to the initial and final state principal

and angular momentum quantum numbers, respectively, ϵ and l' refer to the final state with continuum energy ϵ and angular momentum l'. The energy loss E is related to ϵ by $E=\epsilon-E_{n,1}$, where $E_{n,1}$ is the binding energy of the initial state. The computation of the matrix elements in eq. (2.10) is carried out following Manson (1972), who expanded the operator $\exp(i\vec{K}\cdot\vec{r})$ in terms of spherical Bessel functions which leave a radial integral to be evaluated numerically. The total GOS is obtained from eq. (2.10) by summing over the final angular momentum l' which is determined by the number of partial waves, that is, the number of terms in the superposition of one-electron wave functions required to describe the final state. This number was estimated as follows: The continuum wave function sees an effective potential in eq. (2.8)

$$V_{eff}=V(r)+\frac{l'(l'+1)\hbar^2}{2m_o r^2} \qquad (2.11)$$

For large l', this is dominated by the second term, the *centrifugal potential*. If the continuum energy is less than the *centrifugal potential*, overlap between the initial and continuum states is small and therefore these values of l' will contribute little to the GOS. It was assumed that most of the initial state is contained within a distance a_o (the Bohr radius), where the centrifugal potential is less or approximately equal to ϵ, that is, $[l'(l'+1)\hbar^2/2m_o a_o^2]<\epsilon$. For ϵ=1000eV, typically 10 partial waves were required to describe the continuum wave function. As an example of this

calculation, in figure 2.3a is shown the GOS for transition into the continuum from the 2*p* subshell in Silicon.

The differential cross-section. The differential cross-section, written in terms of the scattering angle, yields a double-differential cross-section which gives the energy differential cross-section per unit solid angle Ω.

$$\frac{d^2\sigma_{nl}(E,\theta)}{dEd\Omega} = \frac{2e^2}{m_o v^2 E} \frac{1}{\theta^2+\theta_E^2} \frac{df_{nl}(E,K)}{dE} \qquad (2.12)$$

where $\hbar^2K^2/2m_oE_o=\theta^2+\theta_E^2$ and $\theta_E=E/2E_o$. The former relation is obtained from conservation of momentum and energy in the scattering process for $E<E_o$ and $\theta<\pi$. E is the energy lost by the incident electron with energy E_o and θ is the scattering angle.

The differential cross-section derived from the GOS by integration of eq. (2.12) up to momentum transfer defined by different angular apertures gives rise to an energy-loss spectrum which may be used to obtain partial or total cross-sections. The energy-loss spectrum was computed within this model up to some hundreds of eV above threshold for selected elements. Some of these results are shown in figure 2.3b.

2.4 TOTAL-INELASTIC CROSS-SECTIONS

The total cross-section for inelastic scattering σ_{in} is defined as the sum of all possible inelastic-collisions which may result from different processes. These processes are generally transitions of ground to excited states,

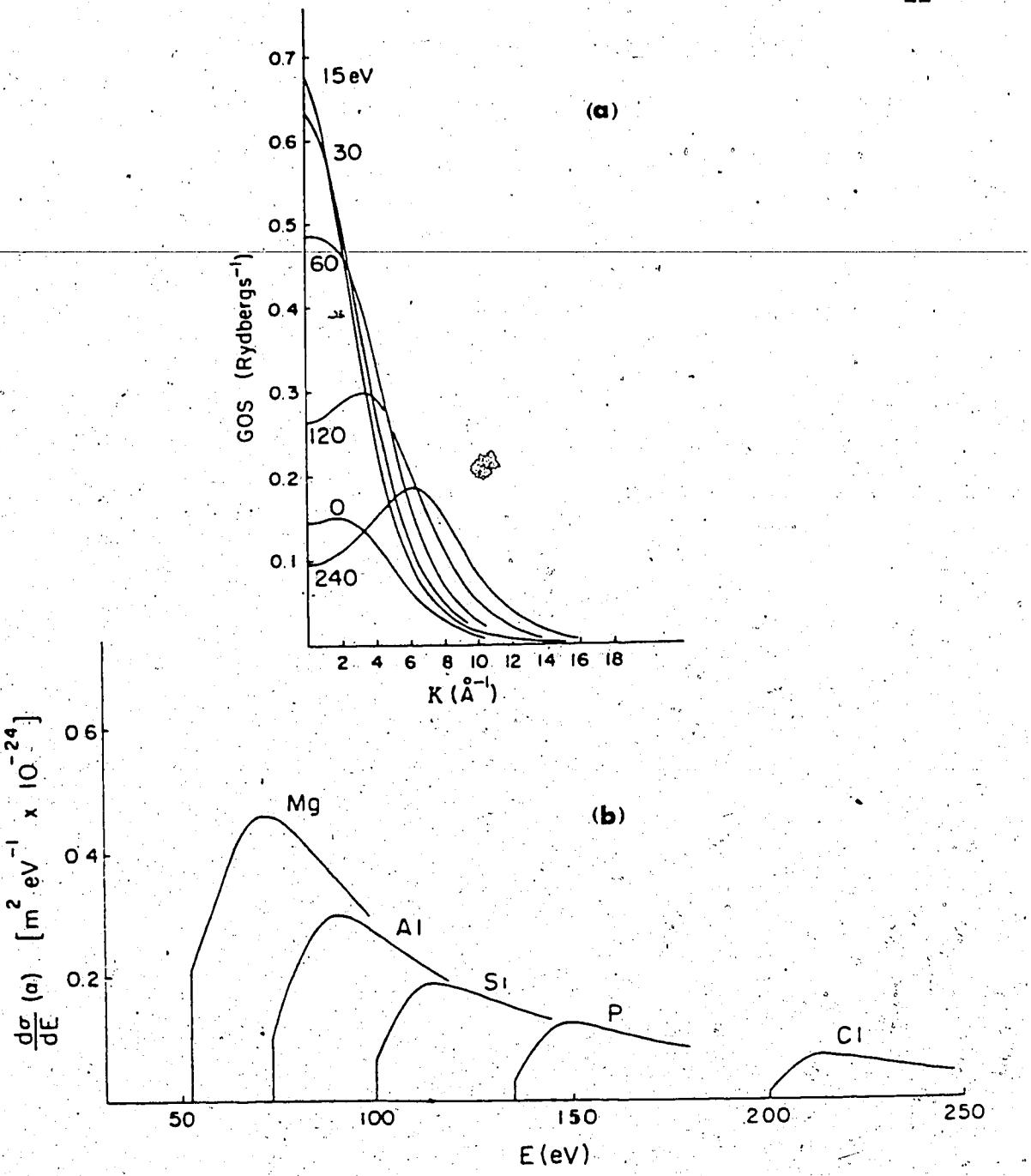

Figure 2.3 (a) GOS for transition into the continuum from 2*p* subshell in Silicon. (b) $L_{2,3}$ edges for 10mrad collection angle for elements in the third period (Leapman *et al* 1980).

including discret and continuum, In this section we present the different atomic models to calculate σ_{in}.

2.4.1 LENZ THEORY

Lenz (1954) has discussed the inelastic scattering of medium-energy electrons by atoms at very small angles (10^{-1} to 10^{-4} radian). By medium energy is meant a range around 100keV, such that relativistic effects are not severe and the first Born approximation can be used. Lenz bases his theory on a simple model of the atom, namely that due to Wentzel (1927). Wentzel express the potential V(r) at radius r of the screened Coulomb field of an atom as

$$V(r)=(Ze/r)\exp(-r/R) \tag{2.13}$$

where R is related to the mean square radius of the atom $\langle r^2 \rangle$ and to a parameter Θ, defined by Lenz in terms of the radial distribution function for the electron cloud around the atom, by

$$R=(\langle r^2 \rangle/6)^{1/2}=(\Theta/6Z)^{1/2} \tag{2.14}$$

In addition, Lenz uses a modification of the elastic scattering theory due to Morse (1932), from which the total inelastic cross-section is given by:

$$\sigma_{in}=(2\lambda^2/\pi a_o)\int_{\bar{q}}^{\infty}\frac{S(q)}{q^3}dq \tag{2.15}$$

where S(q) is the incoherent scattering factor and $\bar{q}$ is a parameter defined by

$$q = \frac{2\pi}{\lambda}\left[\theta^2 + J/(4eV)^2\right]^{1/2} \qquad (2.16)$$

Here J is the first ionization energy of the atom, V and λ are the accelerating potential and wavelength of the incident electron, respectively, and θ is the scattering angle. To define S(q) Lenz uses the Raman-Compton formula $S(q)=Z-F^2/Z$, where F is the x-ray scattering factor. Using a screened Coulomb model [i.e., eq. (2.13)] for F, integration of eq. (2.15) over all q one obtains the total cross-section

$$\sigma_{in}=(\lambda^2\Theta^2/3\pi a_o)\ \ln(6Z/\bar{q}\Theta)=(2\lambda^2\ R^2Z/\pi a_o)\ \ln(1/\bar{q}^2R^2) \qquad (2.17)$$

In fact, this expression results from a small angle approximation; that is, the derivation has made the approximation: $(\bar{q}^2\Theta/6Z)\ll 1$ where $\bar{q}=m_o\lambda J/4\pi\hbar^2$. Lenz indicates that this approximation affects only the angular distribution $\theta<10^{-5}$ at 50 to 100keV.

It is important to point out that the accuracy of this equation depends largely on the atomic properties of the sample, which are present through R and J. To estimate R, it is necessary to consider particular theories of the atom, and Lenz produces, using the Thomas-Fermi model, a general value $R=a_oZ^{-1/3}$. Furthermore, Lenz uses the Hartree self-consistent field to evaluate $Z\langle r^2\rangle$ for C and Cr producing values of 4.64Å² and 5.60Å², respectively. And from Leisegang's (1952) experimental results for Au, Lenz finds $Z\langle r^2\rangle=6.4A^2$. Haine and Agar (1959) have assumed, from the near constancy of the three values of $Z\langle r^2\rangle$ given by

Lenz, that $Z\langle r^2\rangle$ is a constant for all Z and of value about 5Å^2; this assumption corresponds to $R=(\sqrt{3})a_0Z^{-1/2}$. Lately, Langmore *et al.* (1973) based on Hartree-Slater calculations have proposed a value of $R=(0.9)a_0Z^{-1/4}$. In addition, one may define R in terms of the electron scattering factor for zero scattering angle f(0), which is related to the mean square radius of the atom by $f(0)=Z\langle r^2\rangle/3a_0$. Thus, combining this relation and eq. (2.14), one obtains the expression

$$R^2= a_0 f(0)/2Z \qquad (2.18)$$

Using this expression for R and taking the mean excitation energy of the atom I in the place of the first ionization energy J (used by Lenz), one expects more realistic results since f(0) and I have been calculated (Doyle and Turner 1968, Berger and Seltzer 1982, and Turner *et al.* 1979) using accurate wave functions for the atom.

In order to compare our experimental results with predicted inelastic cross-sections based on different atomic models (i.e., different values of the effective radius of the atom), we have done calculations, for different atoms, using eq. (2.17) and the different expressions for R mentioned above. The values for J and I were taken from the literature (Wast and Melvin 1981, Berger and Seltzer 1982); we assumed an energy of 80keV for the incident electrons. The results of these calculations will be presented in Chapter IV for comparison with the experimental results. In figure 2.4 we compare the Lenz theory with other models of

the atom (see below).

2.4.2 TOTAL-INELASTIC CROSS-SECTIONS BASED ON THE HARTREE-SLATER MODEL

Inokuti *et al.* (1975, 1981) have reported values of two parameters involved in the evaluation of the cross-section for inelastic scattering of fast electrons by atoms. Their calculations are based on a single-electron approximation using Hartree-Slater independent-electron wave functions. In addition the first Born approximation is used.

When one integrates eq. (2.1) over all possible values of momentum transfer $\hbar\vec{K}$ for a given excitation energy E corresponding to the state n, one obtains a compact expression called the Bethe cross-section

$$\sigma_n = 4\pi a_o^2 (R/T)\{M_n^2(\ln[\beta^2/1-\beta^2]-\beta^2)+C_n\} \qquad (2.19)$$

This expression is actually the result incorporating relativistic effects, where $\beta=v/c$, a_o, R, and T as defined in section 2.3. The two parameters M_n^2 and C_n are atomic properties derived from the GOS. In particular, M_n^2 is the density of the dipole matrix element and is given by

$$M_n^2 = (R/E)\frac{df}{dE}n \qquad (2.20)$$

C_n being related to M_n^2 by

$$C_n = M_n^2[\ln c_n + 11.2268\ ] \qquad (2.21)$$

Any sum of σ_n over different n values has the same analytical dependence on T and is characterized by two parameters, M_n^2 and C_n. In particular, the total inelastic cross-section, i.e., the sum of σ_n over all n (discrete and continuum energies), may be written as (Inokuti *et al.* 1981)

$$\sigma_{in} = 4\pi a_o^2 (R/T)\{M_{tot}^2(\ln[\beta^2/1-\beta^2]-\beta^2) + C_{tot}\} \qquad (2.22)$$

where the total dipole matrix element square M_{to}^2 is obtained by summing eq. (2.20) over all n, that is: $M_{to}^2=\Sigma_n M_n$. The second quantity in the total cross-section is $C_{to}=M_{to}^2[\ln(c_{to})+11.2269]$. According to the general theory (Inokuti *et al.* 1967) it may be evaluated by means of the ralation $M_{to}^2\ln(c_{to})=-2L(-1)+I_1-I_2$ where L(-1) is a quantity defined by

$$L(-1)= \int (R/E)\ln(E/R)\frac{df}{dE}\,dE \qquad (2.23)$$

and the quantities I_1 and I_2 are integrals containing the incoherent scattering function $S_{in}(K)$ which is an internal state property. These quantities are given by

$$I_1= \int_1^\infty ZS_{in}(K)(Ka_o)^{-4}d(Ka_o)^2 \qquad (2.24)$$

$$I_2= \int_0^1 [M_{tot}^2 - \frac{ZS_{in}(K)}{(Ka_o)^2}](Ka_o)^{-2}d(Ka_o)^2 \qquad (2.25)$$

Thus, $\ln(c_{to})$ can be computed from two items of information, namely, the optical oscillator-strength distribution df/dE and the wave function of the initial state (most commonly the ground state).

Using the values of the parameters, $M^2_{i0,}$ and $M^2_{i0,}\ln(c_{i0,})$, for different elements (Inokuti *et al*. 1975, 1981) we have evaluated eq. (2.22) for 80keV incident electrons. The results are presented in Chapter IV for comparison with the experimental results. In figure 2.4 we compare the Lenz theory with the Hartree-Slater model.

2.4.3 FREE ELECTRON THEORY

It is known from the work of Bohm and Pines (1953) that electrons in a solid can undergo collective or plasma oscillations of fairly defined frequency. For a free-electron plasma the frequency is given by

$$\omega_p = (n_f e^2/m\varepsilon_o)^{1/2} \qquad (2.26)$$

where n is the free electron density in the plasma and m and e the electron mass and charge respectively. If fast incident electrons of energy E_o traverse a sample, they are able to excite quanta of these oscillations, known as plasmons, of energy

$$E_p = \hbar\omega_p \qquad (2.27)$$

In this scattering process the momentum and energy must be conserved. This conservation yields an equation which relates the momentum transfer $\hbar\vec{K}$ to the scattering angle θ of the incident electrons with momentum $\hbar\vec{k}$, as follows

$$K^2 = K_{\parallel}^2 + K_{\perp}^2 \qquad (2.28)$$

Here $K_\perp = k\theta$ and $K_\parallel = k\theta_E$, where $\theta_E = E_p/2E_o$ is the half-width of the angular distribution of these scattered electrons. Typical values of the plasmon energy E_p lie in the range 10-30eV.

The differential inverse mean free path for electrons which suffer a loss E_p has been calculated as a function of the scattering angle θ (Ferrell 1956)

$$\frac{d(1/\lambda_p)}{d\Omega} = \frac{d(n\sigma)}{d\Omega} = \frac{1}{2\pi a_o} \frac{\theta_E}{\theta_E^2 + \theta^2} \qquad (2.29)$$

λ_p is the mean free path for plasmon excitation, its reciprocal value is $n\,\sigma_p$, n being the electron concentration per unit volume and σ_p the cross-section per atom. Integration of eq. (2.29) gives the integral cross-section σ_p for plasmon scattering through any angle up to θ_c

$$\sigma_p = (\theta_E/na_o)\ \ln(\theta_c/\theta_E) \qquad (2.30)$$

Taking calculated values of $\theta_c = k_c/k$ (k_c =critical wave vector and k=wave vector of the incident electron) for different elements at E_o=80keV, the dependence of σ_p on the atomic number Z according to eq. (2.30) is given in figure 2.4. For comparison we include data based on the Lenz and Hartree-Slater models, eqs. (2.17) and (2.22) respectively.

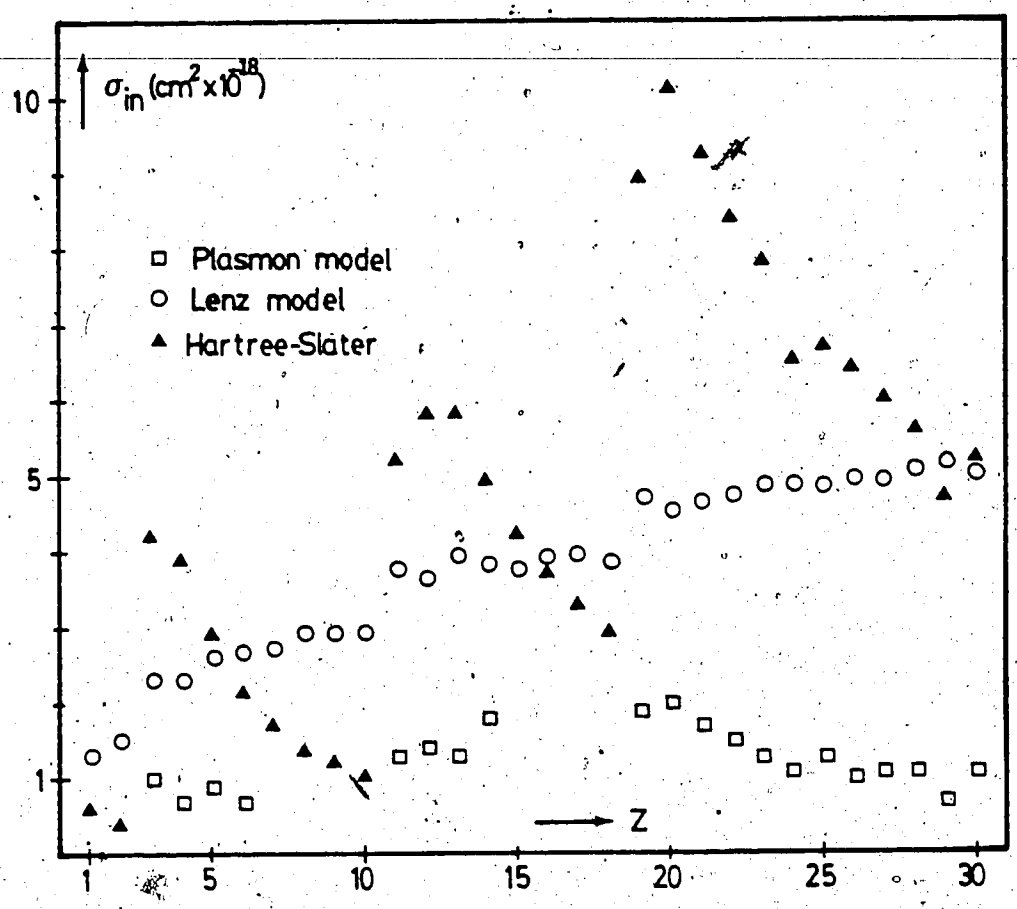

Figure 2.4 Cross-sections for inelastic scattering of 80keV incident electrons. The calculations are based on the Lenz, Hartree-Slater and Plasmon model.

CHAPTER III

EXPERIMENTAL DETERMINATION OF INELASTIC CROSS-SECTIONS

3.1 INTRODUCTION

In the Conventional Transmission Electron Microscope (CTEM) the spectral energy distribution in the transmitted beam, which results from the interaction between the primary electron beam of energy E_0 and the specimen, contains useful information concerning the physical and chemical properties of the sample. The analysis of the energy of these transmitted electrons is in essence a kind of spectroscopy called Electron Energy-Loss Spectroscopy (EELS).

In order to carry out an energy-loss experiment to measure inelastic cross-sections we require (1) a source of electrons, (2) a suitable sample of the material to be studied, and (3) a device (spectrometer) for analyzing the energy of the transmitted electrons. In general, these components can take a variety of different forms, but we are mainly interested in an experimental arrangement which is compatible with the operation of a CTEM. In this case, the source of electrons will be the gun of the microscope and the incident electrons will be assumed to have a well defined energy E_0 (say 80keV). Because we are using a microscope, the incident beam will be capable of being focussed on to a specimen area whose size and position can be controlled, and which can be imaged using the normal optical system of the instrument. The specimen will be a

thin film or section of the material that we wish to study; some of its characteristics will be discussed later in the section 3.2. The spectrometer is placed after the specimen, as shown in figure 3.1, to analyze the transmitted electrons.

All the information that is obtained about the sample is contained in the angular and energy distribution of the electrons that have passed through the specimen. By studying these distributions, resulting from the interaction between the incident electrons and the sample, the required information relating to inelastic cross-sections can be measured. The method used to carry out the analysis is described in the section 3.3. Finally, in the section 3.4 we give some details of the experimental procedure. Some recorded spectra are shown in section 3.4 as well.

3.2 SAMPLE PREPARATION

There are many conditions which the ideal sample should fulfill (i.e., have a clean surface, be homogeneous, etc) and most preparation methods involve a compromise with respect to some of them. The most obvious requirement is that the specimen be transparent to electrons (with and without an objective aperture in place). In other words, that the specimen be thin enough for an electron microscope investigation.

To perform energy-loss experiments we require thin uniform films or sections of known thickness. The specimen

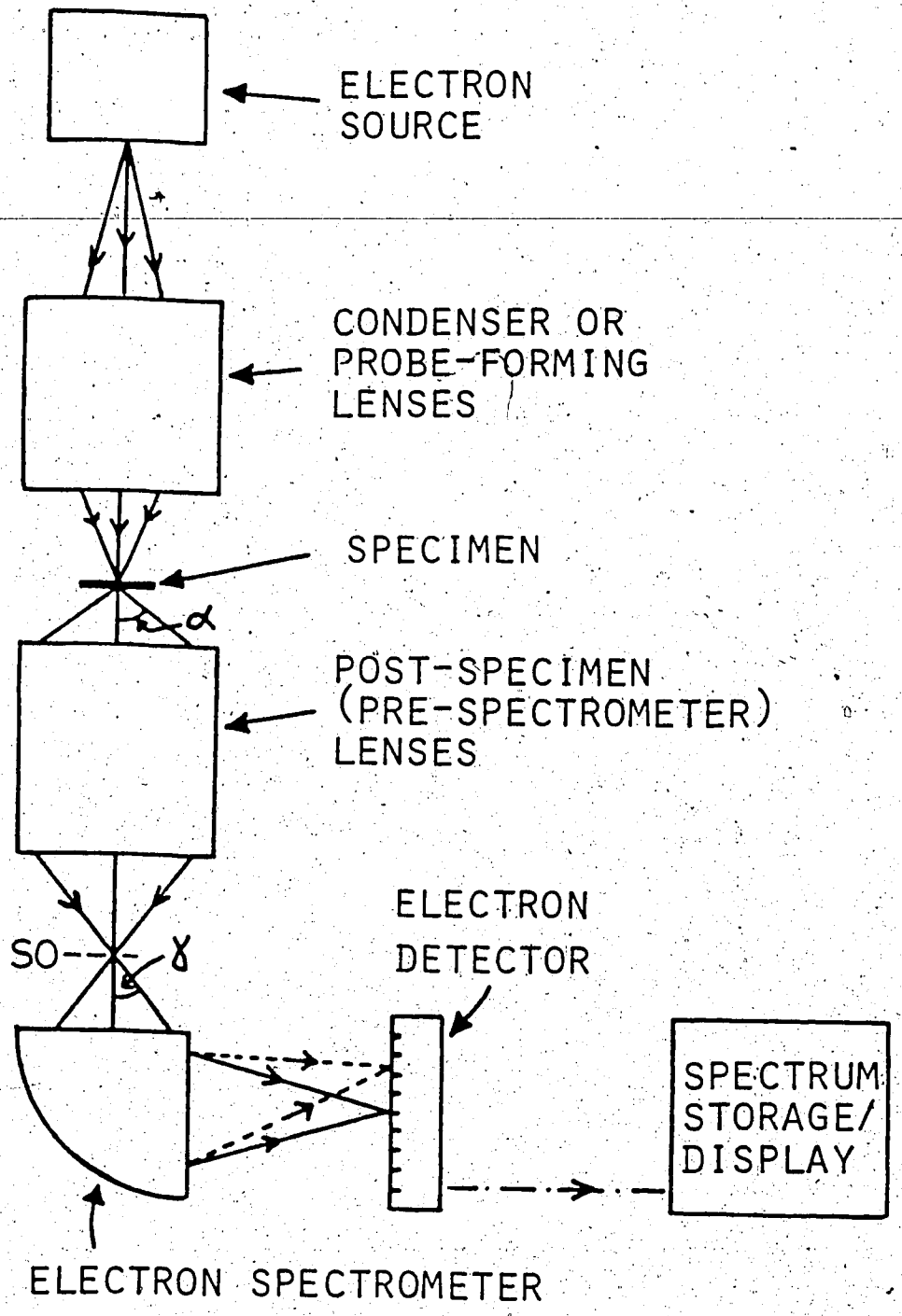

Figure 3.1 Typical EELS system (Egerton 1982).

thickness should in general satisfy the relationship $t<\lambda_{in}/2$ (Zaluzec 1980), where λ_{in} is the total mean free path for inelastic scattering and t the specimen thickness, which for 80keV incident electrons and a typical sample containing light elements (Z<30) is in the range 20-60nm.

3.2.1 VACUUM EVAPORATION

Thin carbon films were evaporated on mica then floated off, on the surface of distilled water, by dipping them under the water and picking them up on 3-mm diameter copper grids (150 mesh per inch). These carbon films were used to support thin polycrystalline metallic films which were prepared by evaporation in vacuo at a base pressure of about 10^{-5} Torr. The film thicknesses of 33nm Aluminum, 28nm Chromium, 24nm Iron, and 48nm Copper were measured using a quartz-crystal thickness monitor situated near the electron microscope grids. Because accurate film thickness measurements are of crucial importance in the present work [see eq. (3.2)] the quartz-crystal monitor was previously calibrated by interferometry (see next section).

3.2.2 THICKNESS MEASUREMENT BY INTERFERENCE MICROSCOPY

One of the important applications of the Light Interference Microscope (LIM) is the measurement of the thickness of films by determination of the height of the step made by the edge of the film when formed on an optically smooth substrate.

The general arrangement shown in figure 3.2 provides the production of interference bands in a LIM. The light from a thallium lamp, after it has been made parallel by the lens, is split in a beam-splitting Prism. A part of the light falls on the Mirror, the other part on the Test Object (TO). The light from both, the Mirror and the TO is reflected back to the beam splitting Prism. There the rays are again united. If one observes from point A, then one can ascertain interference phenomena. If the Mirror and the TO are equidistant from the Prism and if they are not precisely perpendicular to each other, then one sees parallel interference fringes (see figure 3.3a). These fringes result from interference of waves which are delayed from one another by half a wavelength. So the thickness information is obtained by multiplying the interference band shift, in fractions of the band interval, by half the wavelength, i.e.,

$$t = (\lambda/2)\left(\frac{\text{shift}}{\text{band interval}}\right) \qquad (3.1)$$

The band interval is taken as the distance from band middle to band middle, the shift is the "height" of the step made by the edge (see fig. 3.3a), and for thallium light $\lambda/2 = 0.27\ \mu m$.

When measuring the film thickness using a LIM it is desirable to have as sharp edges as possible. For metallic films, one method which was found quite satisfactory is to grow the film with a step, by using a suitable evaporation

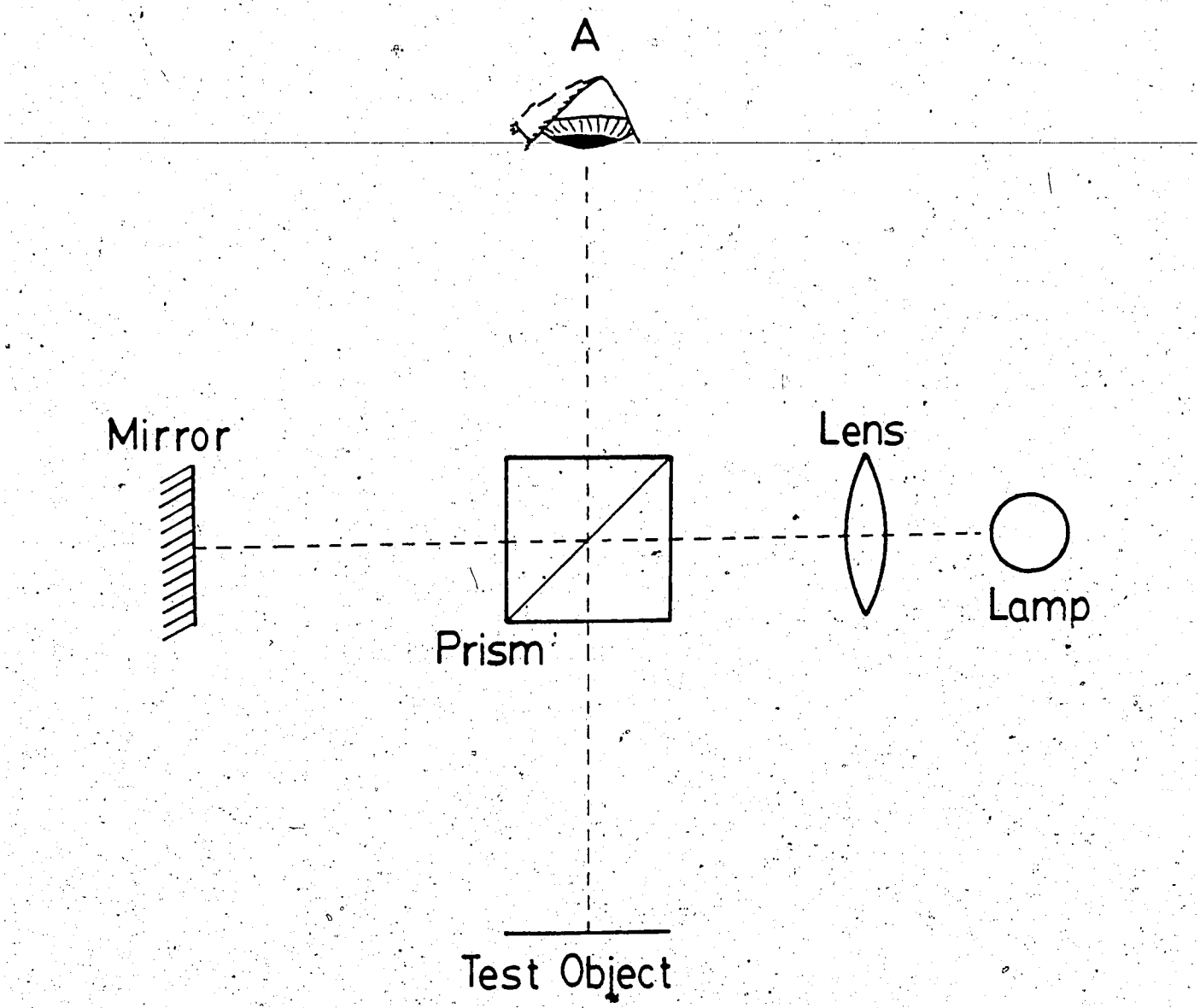

Figure 3.2 A general experimental arrangement for producing interference fringes

mask such as a narrow strip of metal or a thin microscope cover glass. Using this method to form the step, thick metallic films (of the elements studied) that could be measured by interferometry were evaporated, while observing and recording the change in frequency of the quartz-crystal thickness monitor. The films were grown on standard microscope slides, then mounted on the table of the LIM. A picture of the fringes observed is given in figure 3.3a. In figure 3.3b we show (as an example) the quartz-oscillator calibration curve for Copper, assuming the thickness predicted by the eq. (3.1) and Copper density ρ=8.9g/cm^3. For the other elements studied similar results were obtained.

3.3 COLLECTION AND ANALYSIS OF AN ENERGY-LOSS SPECTRUM

To characterize the interactions of the incident electrons and the sample we collect all the transmitted electrons lying within a cone of some semi-angle α (in a CTEM this angle is limited by an objective aperture located on the back focal plane of the objective lens) about the incident beam direction, and then analyze these for their energy loss. The result that we obtain from such an experiment is an energy-loss spectrum (ELS), in which we plot the transmitted signal intensity I as a function of the energy-loss E for all the electrons scattered within the angular cone α accepted by the spectrometer. Figure 3.4 shows schematically an ELS. The spectrum consists of:

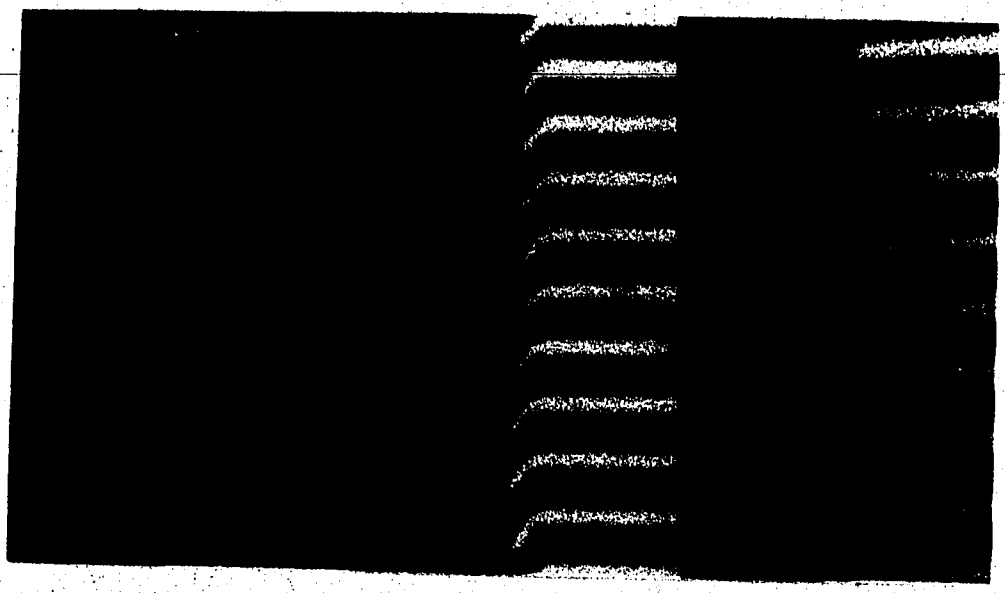

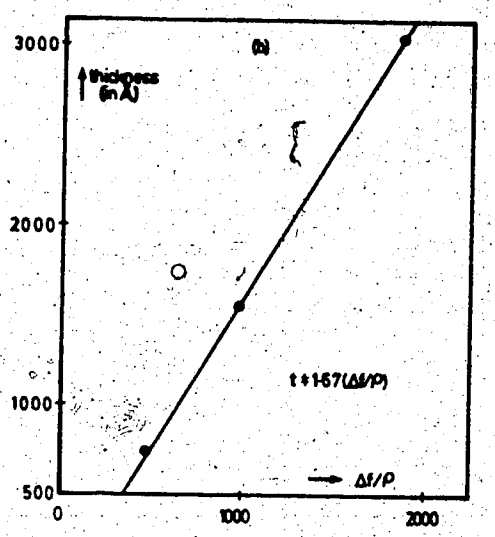

Figure 3.3 (a) Interference fringes showing the shift measured to obtain the thickness of the copper films, (b) calibration curve for the quartz-crystal thickness monitor.

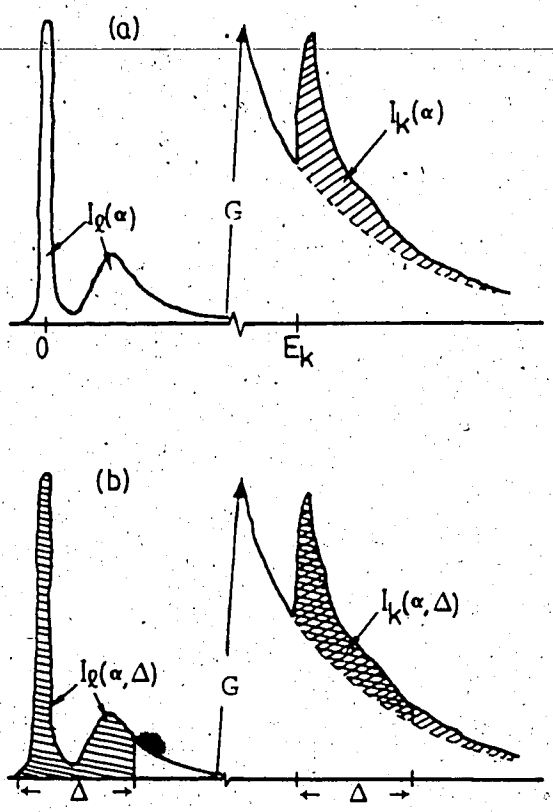

Figure 3.4 Schematic Energy-Loss Spectrum (a) shows the low-loss region and a characteristic edge (b) shows the areas $I_1(\alpha,\Delta)$ and $I_k(\alpha,\Delta)$.

(1) A sharp peak at E=0 representing the elastically scattered and unscattered electrons from the incident beam (one normally refers to this as the zero-loss peak).

(2) A broad peak in the range E=10 to 40eV indicating energy loss due to excitation of plasmons or valence-electron transitions. These two peaks lie in the region of the spectrum known as the low-loss region.

(3) An abrupt rise in the transmitted intensity representing excitation of inner shell electrons to vacant states in the continuum. This rise, in the high-loss region of the spectrum, takes place above an energy loss equal to the binding energy E_k, where k is the type of inner shell excited (k=K, L, M, etc.), E_k being characteristic of each element in the periodic table of elements.

3.3.1 MEASUREMENT OF IONIZATION PARTIAL CROSS-SECTIONS

The excitation edges in the ELS are normally used to identify the presence of a given element within the area of specimen defined by the incident beam of electrons. A quantitative estimation, giving the number N of atoms of the element per unit area of specimen, is obtained from the area $I_k(\alpha,\Delta)$ measured directly under an excitation edge, after extrapolating and subtracting the background which precedes the edge (see fig. 3.4b). In such a case, the formalism due to Egerton (1978a) can be used to obtain the concentration N of a given element, i.e.,

$$N = \frac{1}{G}\left[\frac{I_k(\alpha,\Delta)}{I_1(\alpha,\Delta)}\right] \frac{1}{\sigma_k(\alpha,\Delta)} \qquad (3.2)$$

here $I_1(\alpha,\Delta)$ is an area measured from the low-loss region of the spectrum (see fig. 3.4b) and $\sigma_k(\alpha,\Delta)$ is a partial cross-section of the element, corresponding to inner-shell losses between E_k and $E_k+\Delta$. The factor G allows for any difference in the detector gain between the low- and the high-energy region of the spectrum.

There are two methods, direct and indirect, in which eq. (3.2) can be used to obtain partial ionization cross-sections. The direct method (used for elements) involves knowledge of the concentration N per unit area of the specimen. This quantity is known if one takes the bulk density ρ of the element and assumes a specimen thickness t, since N is related to the concentration per unit volume n by $N=nt=\rho N_o t/A$, where A is the atomic weight of the constituent atoms and N_o the Avogadro's number. Knowing N, it is pssible to obtain the partial cross-sections from the same measurable quantities mentioned above [i.e., $I_k(\alpha,\Delta)$ and $I_1(\alpha,\Delta)$]. The indirect method (used for stoichiometric compounds) assumes, according to the stoichiometry, the relative abundace N_1/N_2 of two elements in a compound. In this case the ratio of two partial cross-sections $\sigma_{k1}(\alpha,\Delta)$ and $\sigma_{k2}(\alpha,\Delta)$ can be obtained if two excitation edges in the same spectrum are measured under the same conditions, i.e., with the same α and Δ. $I_1(\alpha,\Delta)$ and G in eq. (3.2) cancel giving

$$\frac{\sigma_{k1}(\alpha,\Delta)}{\sigma_{k2}(\alpha,\Delta)} = \frac{N_2}{N_1}\left[\frac{I_{k1}(\alpha,\Delta)}{I_{k2}(\alpha,\Delta)}\right] \qquad (3.3)$$

where $I_{k1}(\alpha,\Delta)$ and $I_{k2}(\alpha,\Delta)$ are the quantities to be measured in the ELS. It is important to point out that the ratio N_1/N_2 is independent of the specimen thickness.

Measurement of Areas in the ELS. The area $I_1(\alpha,\Delta)$ under the low-loss energy region of the spectrum is obtained by straightforward summation of the channel counts. For measurements on inner-shell ionization edges, the background due to other loss processes has to be stripped. The general method for background stripping is to define before the threshold energy E_k a fitting region of interest, or fitting window, which is typically 50 to 200 eV wide and where a power law AE^{-r} (Egerton 1975) is adjusted to the data. To determine A and r we have used the folowing formulae (Egerton 1980):

$$A = (I_1 + I_2)(1 - r)/(E_2^{1-r} - E_1^{1-r}) \qquad (3.4)$$

$$r = 2\log(I_1/I_2)/\log(E_2/E_1) \qquad (3.5)$$

where the fitting window $[E_1,E_2]$ is divided in two halves (see fig. 3.5) of respective integrals I_1 and I_2. Once the fit is made, the power law AE^{-r} is extrapolated under the characteristic edge (see fig. 3.5) up to few hundreds of eV. The area $I_k(\alpha,\Delta)$ is then evaluated using the relation

$$I_k(\alpha,\Delta) = \int_{E_2}^{E_k+\Delta} J(E)dE - \frac{A}{1-r}\left[(E_k+\Delta)^{1-r} - E_2^{1-r}\right] \qquad (3.6)$$

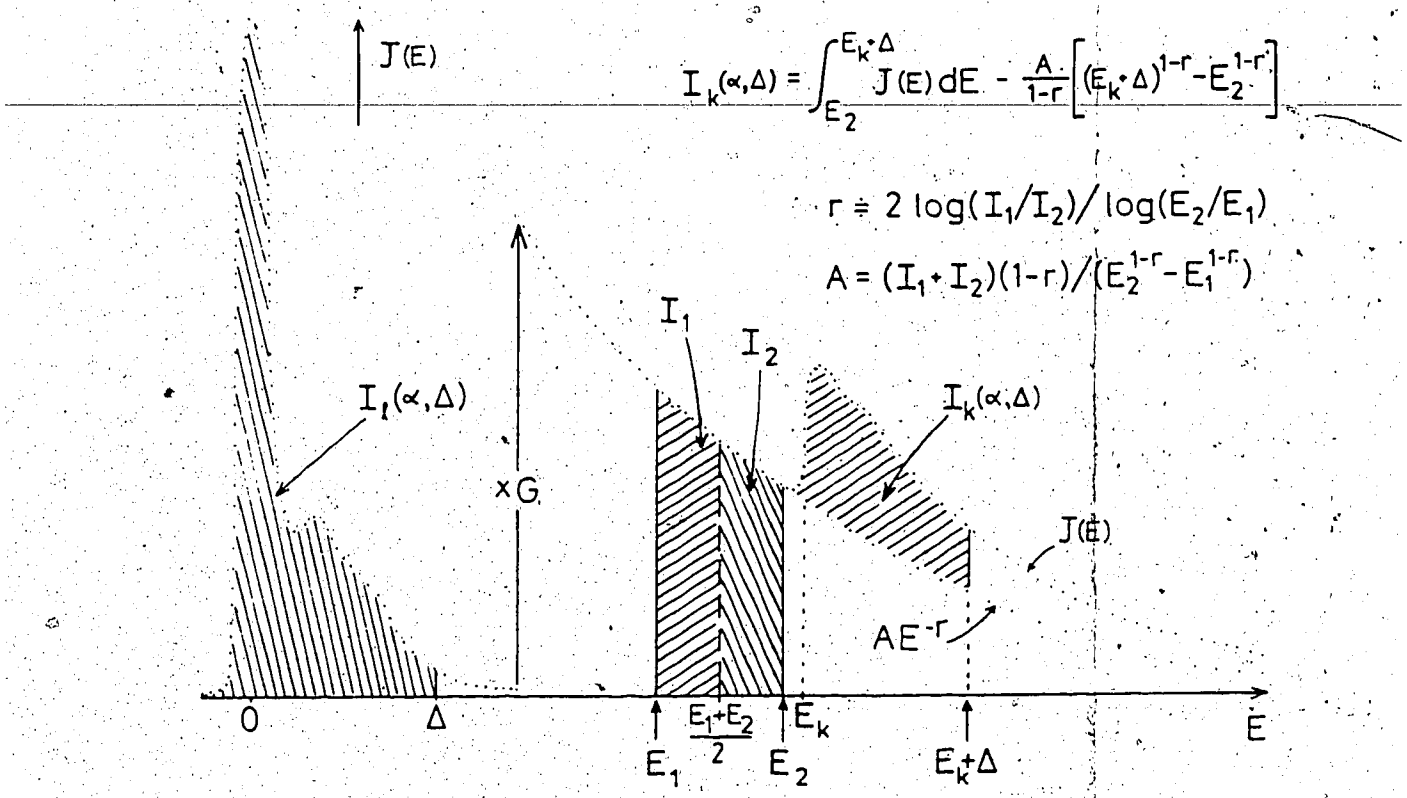

Figure 3.5 Schematic ELS, illustrating measurement of areas for use in eq. (3.2) and the method, described in the text, of background fitting (Egerton 1980).

3.3.2 MEASUREMENT OF TOTAL-INELASTIC CROSS-SECTIONS

The area I_o under the zero-loss peak, relative to the total area I_T under the energy-loss spectrum, can be used for measuring the total mean free path for inelastic scattering λ_{in}, according to the equation

$$\frac{t}{\lambda_{in}} = \ln(I_T/I_o) \qquad (3.7)$$

If the thickness t is known one can find λ_{in} by measuring I_o and I_T. These two quantities are obtained by straightforward summation of the channal counts corresponding to the zero-loss peak and to the total spectrum (typically recorded up to 2000eV for analysis of light elements). The total inelastic cross-section per atom is found using the relation $\sigma_{in}=1/n\lambda_{in}$, where n is the concentration of atoms per unit volume of specimen.

3.4 EXPERIMENTAL DETAILS

The experimental system for recording the energy loss spectrum has been described previously (Egerton 1979). This consists of a JEM 100B transmission electron microscope combined with a custom-made magnetic spectrometer (Egerton 1978b). Using the electron microscope in the diffraction mode, a spot diameter of about 4μm at 80keV primary electrons is incident on the specimen. The transmitted electrons lying in a cone of some width α are focussed on the object plane of the spectrometer by means of an intermediate lens of the microscope operated in

"high-resolution diffraction" mode (in this mode the projector lens is switched off). The electron spectrometer produces its energy dispersion by applying to the transmitted electrons a magnetic field. Spectra are recorded by scanning the exit beam of the spectrometer across an adjustable slit located at the spectrometer image plane, causing electrons of a particular energy loss to fall onto a transmission phosphor screen with a resulting voltage at the output of the photomultiplier tube.

In the present experiments, objective apertures (OA) subtended scattering angles (α) of 6.1, 8.96, and 13.6 mrad were measured using an Aluminium diffraction standard whose diffraction pattern (DP) was recorded on an electron micrograph, figure 3.6. The radius, R_{hkl}, of each ring appearing in the DP is given by

$$R_{hkl} = \frac{\lambda L}{d_{hkl}} \qquad (3.8)$$

where the diffraction constant of the microscope λL (λ=electron wavelength, L=effective distance of the specimen from the screen or plate) is found by mesuring R_{hkl}, directly on the DP (fig. 3.6). The distance, d_{hkl}, between adjacent planes which have diffracted the electrons and originated the rings in the DP is found using the relationship for cubic structures, since Aluminum crystalizes in cubic system, i.e.,

$$d_{hkl} = \frac{a}{(h^2+k^2+l^2)^{1/2}} \qquad (3.9)$$

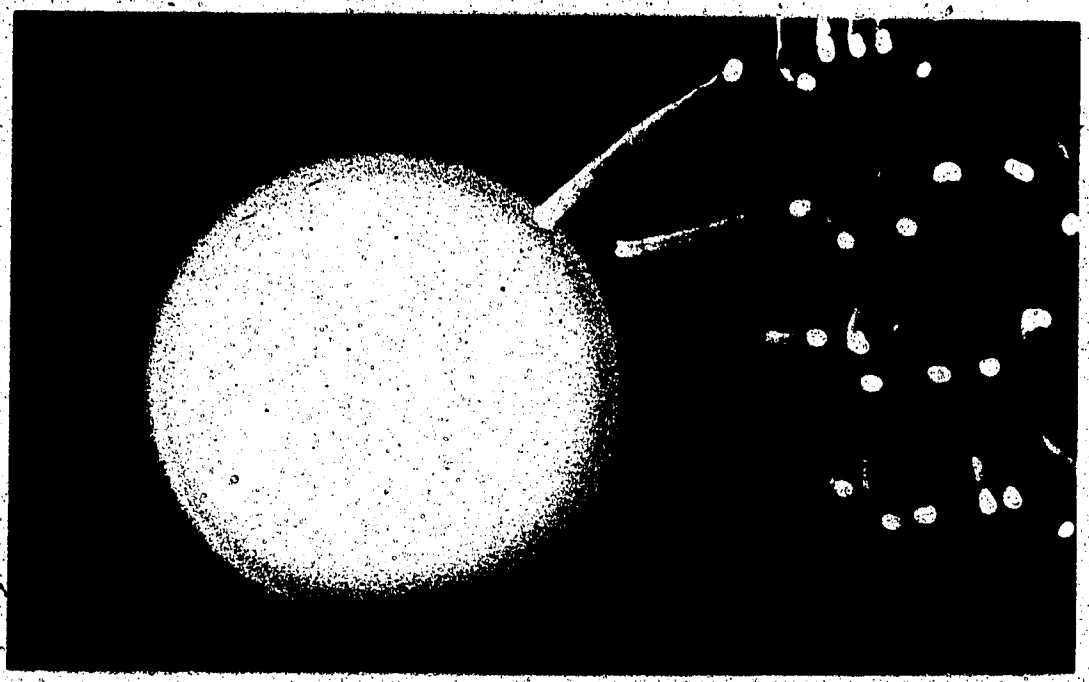

Figure 3.6 Standard diffraction pattern of an Aluminum film used to calibrate the objective apertures of the JEM 100B microscope.

a is the crystal cube edge and h, k, and l are the Miller indices. To estimate α, the objective apertures are inserted and centered, thus superimposed on the Aluminum DP and recorded on photographic plates; by measuring the radius R of the apertures, we are able to find α by means of the relationship

$$\alpha = \frac{R}{L} \tag{3.10}$$

The α values mentioned above are actually averages from three different calibration experiments.

It is important to point out that the Carbon film, used for supporting the metallic films, contributes to the ELS. This contribution is directly reflected in the absolute value of the total-inelastic cross-section. So it is necessary to make corrections for this contribution. The actual quantity that we measure (see section 3.3.2) is due to both the metallic and Carbon film. If we measure (in a separate experiment) the same quantities on a Carbon film the desired (corrected) quantity is given by

$$\left(\frac{t}{\lambda_{in}}\right)_{\text{metallic film}} = \left(\frac{t}{\lambda_{in}}\right)_{\substack{\text{metallic film} \\ \text{on Carbon}}} - \left(\frac{t}{\lambda_{in}}\right)_{\text{Carbon}} \tag{3.11}$$

Using this relationship to make corrections for those metallic films that are supported by Carbon, the total-inelastic cross-section is obtained as described in sectin 3.3.2.

The spectra are acquired in 1024 channels, of a TN-1710 Multichannel Analyzer (MCA), using a typical dwell time (the

time for which the data is stored in each channel) of approximately 40 msec. After acquisition the data is processed with the help of a TN-1117 Floppy disk memory system (used for recording spectra, and loading the system operating program when necessary). This is controlled by a Texas Instruments Silent 700 data terminal, which contains an alphanumeric keyboard and a silent printer. In figure 3.7 recorded spectra are shown for the different elements analyzed. The experimental inelastic cross-sections will be given in Chapter IV for comparison with the theory presented in Chapter II.

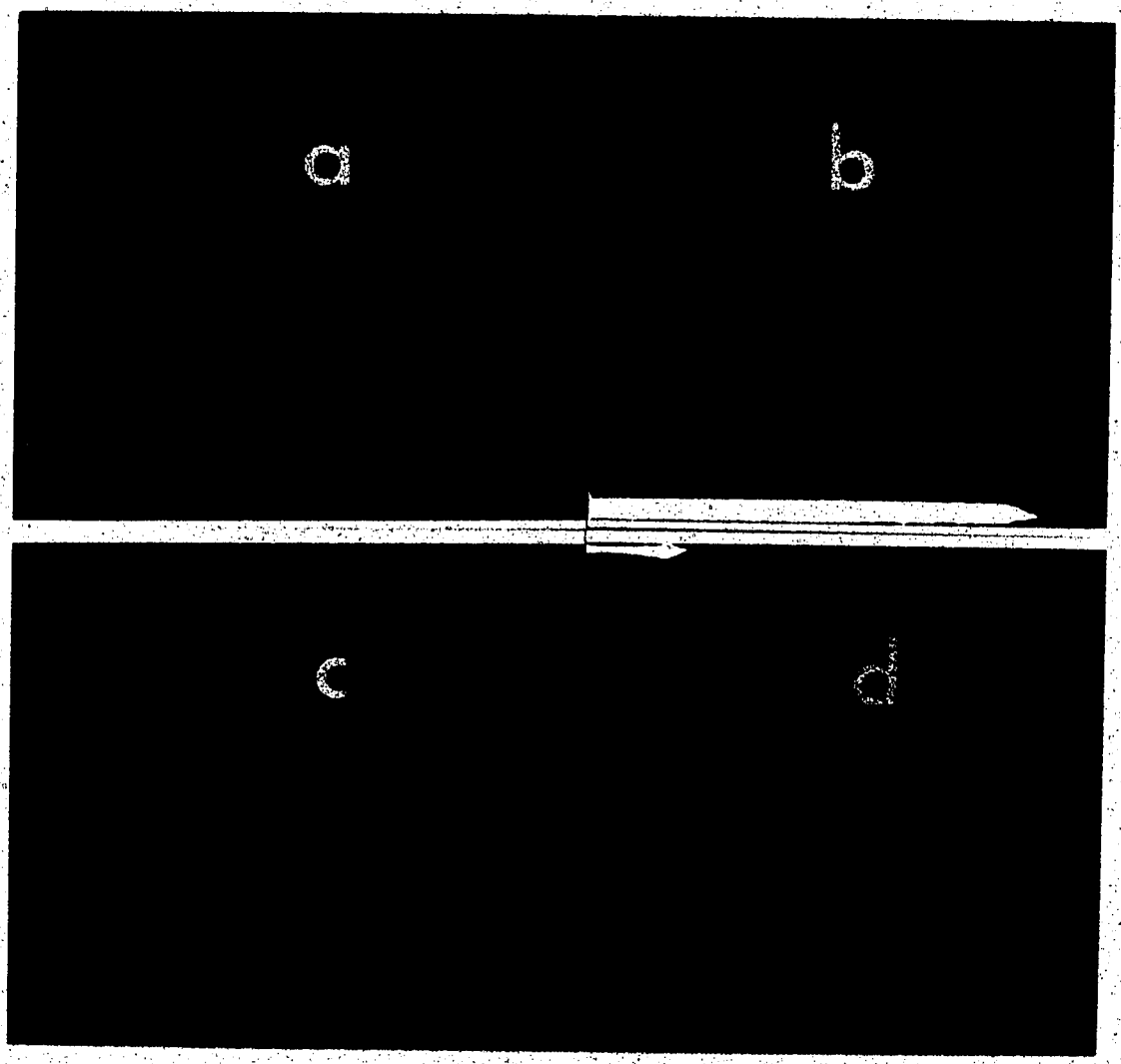

Figure 3.7 Recorded spectrum from (a) a 33nm thick Al film, (b) a 28nm thick Cr film, (c) a 24nm thick Fe film, and (d) a 48nm thick Cu film.

CHAPTER IV

COMPARISON BETWEEN CALCULATED AND EXPERIMENTAL CROSS-SECTIONS

4.1 INTRODUCTION

In Chapter II the different models for calculating inelastic cross-sections were presented. In this Chapter we will compare the results of calculations based on these models with experimental measurements carried out for selected elements (i.e., Al, Cr, Fe, and Cu).

4.2 PARTIAL IONIZATION CROSS-SECTIONS

The cross-section for excitation of atomic electrons from the K-shell in Al, and from the L-shell in Cr, Fe, and Cu is shown, as a function of the collection angle, in figures 4.1 to 4.4. In these figures, the hydrogenic calculations are compared with experimental measurements. For all the elements studied, the experimental measurements show, within the experimental standard deviation, a similar trend as the hydrogenic calculations. This similarity indicates that the hydrogenic model predicts well the angular distribution of the scattered electrons which have excited inner-shell atomic electrons. A similar comparison with the Hartree-Slater calculations is not possible, due to the lack of published data. However, the angular distribution predicted by the Hartree-Slater model can be obtained from eq. (2.12); this equation shows that $d^2\sigma/dEd\Omega$

is proportional to $1/\theta^2+\theta_E^2$ (where $\theta_E = E/2E_0$ and θ the scattering angle). By integrating $d^2\sigma/dEd\Omega$ over a unit of solid angle $d\Omega$, it can be seen that $d\sigma(\alpha)/dE$ is proportional to $\ln[1+(\alpha/\theta_E)^2]$. In fact, this results from small a angle approximation which can be justified because we are in the dipole region (momentum transfer $\hbar\vec{K}=0$). Calculations carried out for Al showed that the Hartree-Slater model predicts a similar angular distribution as that predicted by the hydrogenic model. In figure 4.2 we compare a single calculation based on this model with the experiment. Agreement is closer than with the hydrogenic value, which may be a result of the more accurate wave functions used for calculating the GOS.

Figures 4.1 to 4.4 show the partial ionization cross-sections (for K-shell excitation in Al, L-shell excitation in Cr, Fe, and Cu) integrated up to two different energy windows Δ=100 and 200eV. In these figures we compare the hydrogenic calculations with the experimental data. On the one hand, the experimental values do not lie consistently below or above the values predicted by the hydrogenic calculations (*cf.* figures). This inconsistency can be attributed to the fact that the hydrogenic model does not predict well the shape of the edge near the threshold. For example the L-edge for Cr shows a slight peak at the threshold (see fig. 3.7) which is presumably due to excitation of electrons from the 2p-subshell to the partially filled 2d-subshell. This peak at the threshold

contributes to the partial ionization cross-section, so we expect the experimental measurements to lie above the hydrogenic calculations, as observed in figure 4.2. For the other elements studied (i.e. Al, Fe, and Cu) the edges are not peaked at the threshold (see fig. 3.7) and the experimental values lie below the hydrogenic calculations. That is, the hydrogenic model predicts slightly high values for the cross-section. On the other hand, when the partial ionization cross-sections for L-shell excitation (both experimental and hydrogenic) are integrated up to an energy window Δ=200eV, the agreement between the experiment and theory becomes better (see figure 4.2 to 4.4). The disagreement for small energy window (Δ<200eV) might be expected; since the hydrogenic model in its basic form predicts too large a cross-section near the edge, the program used for calculating the cross-section for L-shell excitation adds an extra energy dependence to the GOS, to bring this in to agreement with X-ray absorption measurements. If this modification is not exact, the percentage error is less for larger energy window. For the elements studied the hydrogenic model agrees , within the experimental standard deviation, with the experiment for an energy window Δ=200eV.

It is relevant to point out that the error bars shown along with the experimental values represent the experimental standard deviation calculated from 10 separate meaurements on each element studied. In addition, it is

important to discuss possible sources of systematic error which could affect our results. First, there may be a systematic error arising from the thickness measurement. This error is estimated to be about 5%. Secondly, error may arise both from the instrument itself and from the experimental procedure.

The instrumental contribution depends on two experimental parameters involved in our measurements. These are the accelerating voltage and the collection semi-angle α. One error associated with the accelerating voltage is instability of the high voltage supply; however, drift would be detectable by the spectrometer. Another effect is that the value E_0 may be different from the stated value. The contribution due to α depends on the uncertainty of the measurement of α itself, and also on the particular excitation of the objective lens. In our situation, where the specimen is properly focussed and the film specimen is always at same high (as observed from the focus current), this contribution is mainly due to calibration error and is estimated to be less than 10%. The procedural error depends on the quantitation formula [eq. (3.2)] used for carrying out the analysis. This formula underestimates contributions from Bragg-scattered electrons just outside the objective aperture (which contibute to the characteristic-edge signal and not to the low-loss region). In extreme cases, this procedural error may be as high as 20% (Egerton 1978a).

4.3 TOTAL-INELASTIC CROSS-SECTIONS

In figures 4.5a and 4.5b the total-inelastic cross-section based on the Lenz theory and different expressions for R (the effective radius of the atom) is shown, as a function of the atomic number (Z), for comparison with the experimental data (all the experimental data was obtained using a collection semi-angle α=8.96mrad). For the elements [illegible] the experimental values do not agree consistently (the experimental error) with any of these curves.

However, the experimental value for Cr agrees well with the calculations done using $R=_0Z^{-1/3}$ and $R=(\sqrt{3})a_0Z^{-1/2}$; this good agreement could be because these expressions for R are based on data calculated for Cr.

For Cu, three of the calculations give values fairly close to the experimental one (see figure 4.5). However, all the calculations shown in this figure predict too large a cross-section for Al. This large discrepancy is attributed to solid state effects which are extreme in a case like Al (see discussion below).

On the other hand, the experimental value for Fe lies above the calculated values. This higher measured value is presumably due to an oxide contribution, since Fe oxidizes very easily. The effect of an oxide would be to increase the measured cross-section, by an amount depending on the thickness of the oxide layer.

All these Lenz-model calculations predict a different Z-dependence, but all reflect the shell structure of the atom, which can be clearly seen from figure 4.5 (*cf.* change in slope from Z=2 to 3, Z=10 to 11, etc). We believe that the dependence of the total-inelastic cross-section on the atomic number (Z) should be predicted most accurately by calculations which use the expression $R=a_0 f(0)/2Z$, since the Z-dependence predicted by these calculations is very similar to that predicted by more sophisticated calculations (*cf.* Hartree-Slater calculations in figure 4.6).

In figure 4.6 the cross-sections for inelastic scattering, based on the Plasmon and Hartree-Slater models, are shown as a function of the atomic number (Z), for comparison with the experimental measurements. The experimental values for Cr, Fe, and Cu are all greater than predicted by Plasmon calculations, whereas for Al this model gives the best agreement. This good agreement is nodoubt because Al is more like a free-electron metal than the other metals, as can be seen from the fact that the experimental plasmon energy (16eV) is approximately equal to that predicted by the free-electron plasmon theory (15.8eV). For the other elements the energy difference is appreciable (e.g. for Cr 18.5 and 27 eV, for Fe 16.7 and 23eV respectively) so we might expect the cross-section to be given more accurately by the Hartree-Slater model, as in fact is observed in figure 4.6. For Al, the experimental value is a factor of 2.6 less than predicted by

Hartree-Slater calculations. This large discrepancy is probably due to solid-state effects, which shift the oscillator strength to higher energy loss. This shift can be seen from the fact that in a single Al atom the ionization energy is 5.99eV, whereas in the solid the plasmon energy is approximately 16eV. The energy shift decreases the cross-section, since $d\sigma/dE$ is proportional to $(1/E)df/dE$ [*cf.* eq. (2.1)].

4.4 CONCLUSIONS AND SUGGESTIONS FOR FURTHER WORK

In this section some conclusions of this thesis are summarised and suggestions made as to how the work presented could be continued.

Comparison between the hydrogenic model and experiment indicates that for all the elements studied the former predicts well the angular distribution of the scattered electrons which have excited inner-shell atomic electrons. Although these measurements were carried out only for a few elements, we might expect similar results for other elements. The comparison also indicates that the hydrogenic model is less accurate for calculating L-shell cross-sections with low energy windows ($\Delta<200$eV). This discrepancy between theory and experiment may be due to both atomic and solid-state fine structure near the edge. On basis of the present experimental results this effect was found to be less for a large energy window ($\Delta=200$eV).

It would be interesting to extend the study to other elements like Ti and Ni to complete the study of the 3*d* transition metals. Also it would be useful to carry out measurements on their respective oxides, which have a different solid-state fine structure than the metals.

Comparison between the different models for calculating total-inelastic cross-sections and experiment indicates that no single model predicts well the cross-section. However, the cross-section for metals whose valence losses are mainly due to single-electron transitions should be predicted more accurately by atomic models. Furthermore, for metals (like Al) whose valence losses are mainly due to collective excitations, the cross-section should be predicted more accurately by the plasmon free-electron theory.

It would be useful to extend the study to other free-electron metals (like Mg, Ca, and In) to test the above statement. It is also necessary to extend the experiments to test the accuracy of the atomic models.

Because the Hartree-Slater calculations are presumably more realistic, we would expect best predictions from these calculations; but on basis of the present experimental results, this cannot be confirmed. So it would be interesting to carry out measurements for other elements (e.g. Ti, Co, Ni, etc). Also it would be advantageous to extend measurements to higher α to enable direct comparison with total-inelastic cross-sections.

For estimating the local thickness t of a specimen, by means of eq. (3.7), it would be convenient to have a model for calculating the required mean free path for inelastic scattering. On the basis of the present experimental results the mean free path for free-electron metals (e.g. Mg, Ca, In, Sn, Cs, and Rb) can, in principle, be estimated using the plasmon free-electron theory. For elements like Cr, Fe, and Cu the mean free path can be estimated using the Hartree-Slater or the Lenz model with $R=a_0 f(0)/2Z$. However, in many cases (e.g. compounds and organic substances) it is not obvious which model is more appropriate. In this case one must rely on experimental measurements of the inelastic mean free path.

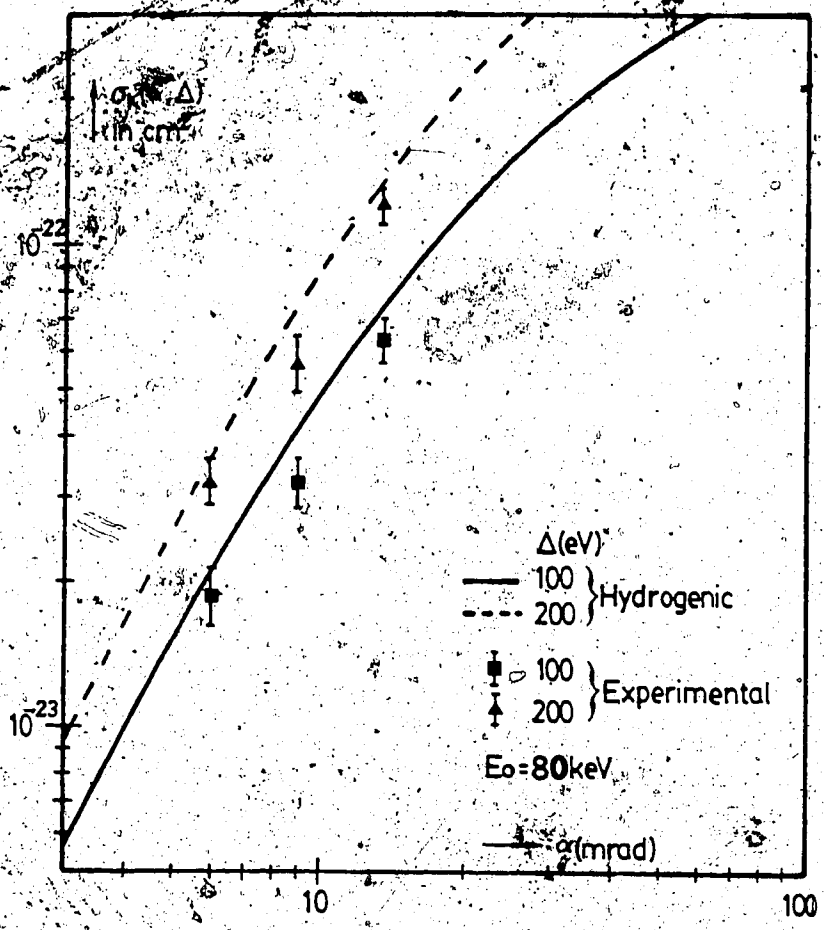

Figure 4.1 Hydrogenic and experimental cross-sections for K-shell excitation in Al as a function of collection semi-angle α, for 80keV incident electrons.

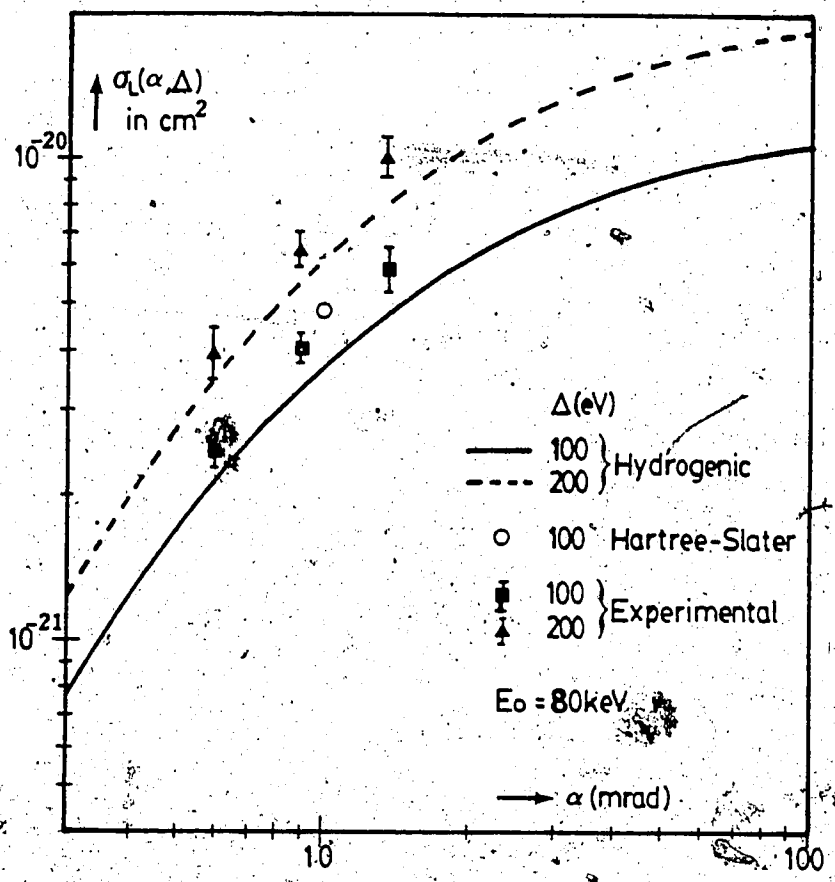

Figure 4.2 Hydrogenic, Hartree-Slater, and experimental cross-sections for L-shell excitation in Cr as a function of collection semi-angle α.

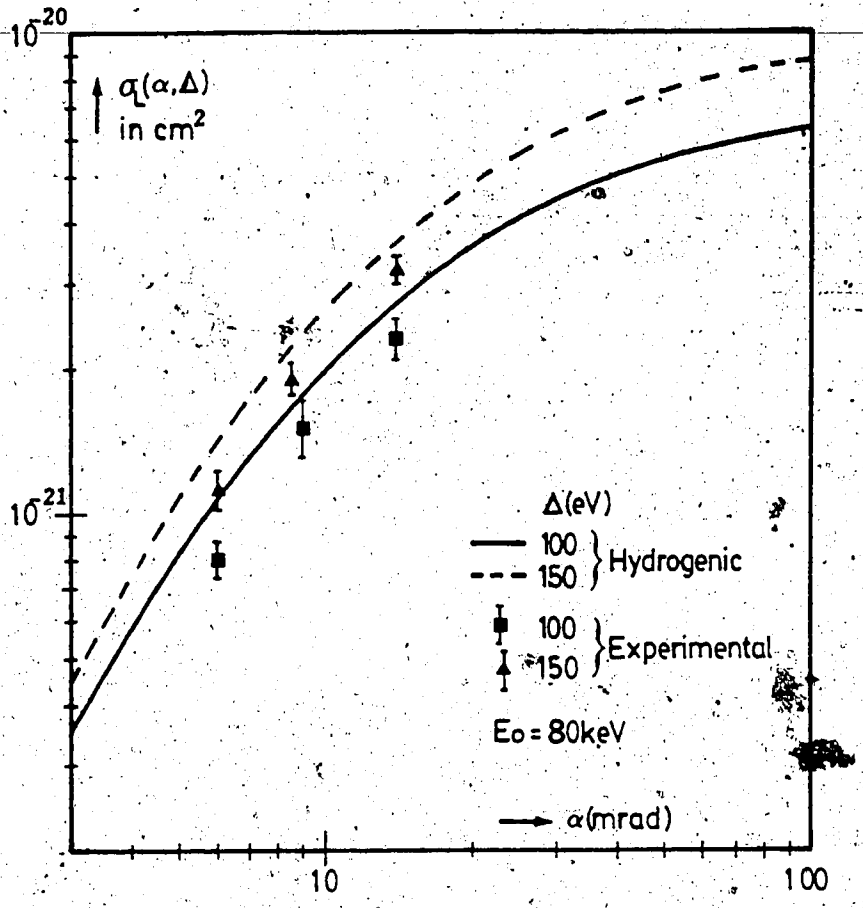

Figure 4.3 Hydrogenic and experimental cross-sections for L-shell excitation in Fe as a function of collection semi-angle α, for 80keV incident electrons.

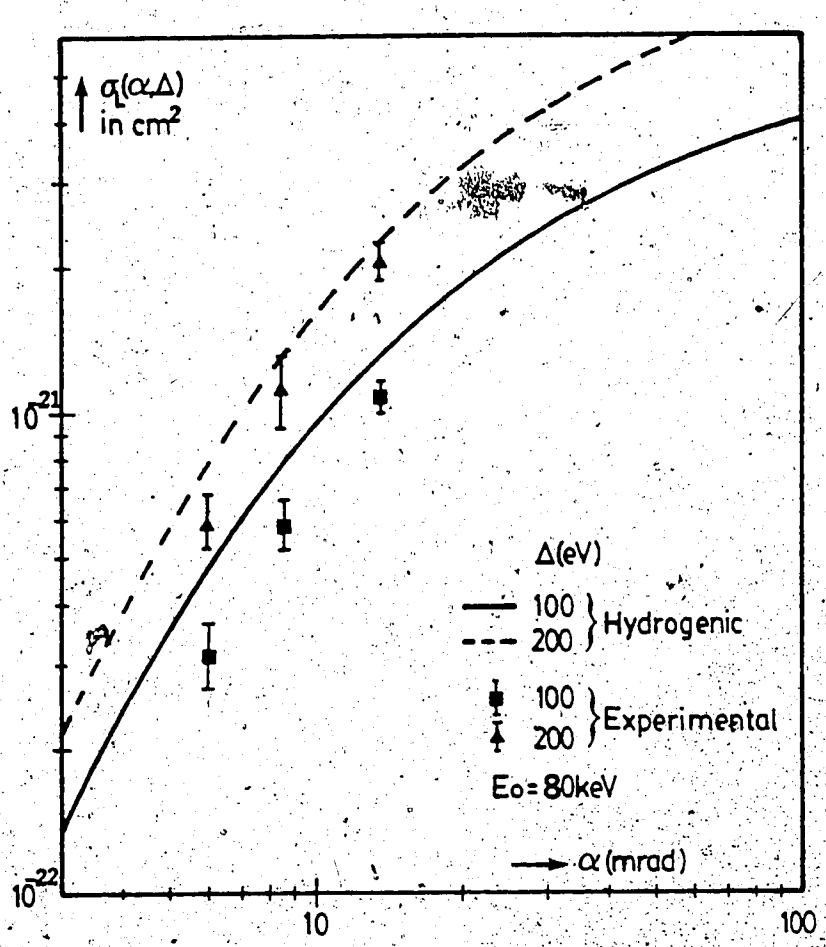

Figure 4.4 Hydrogenic and experimental cross-sections for L-shell excitation in Cu as a function of collection semi-angle α, for 80keV incident electrons.

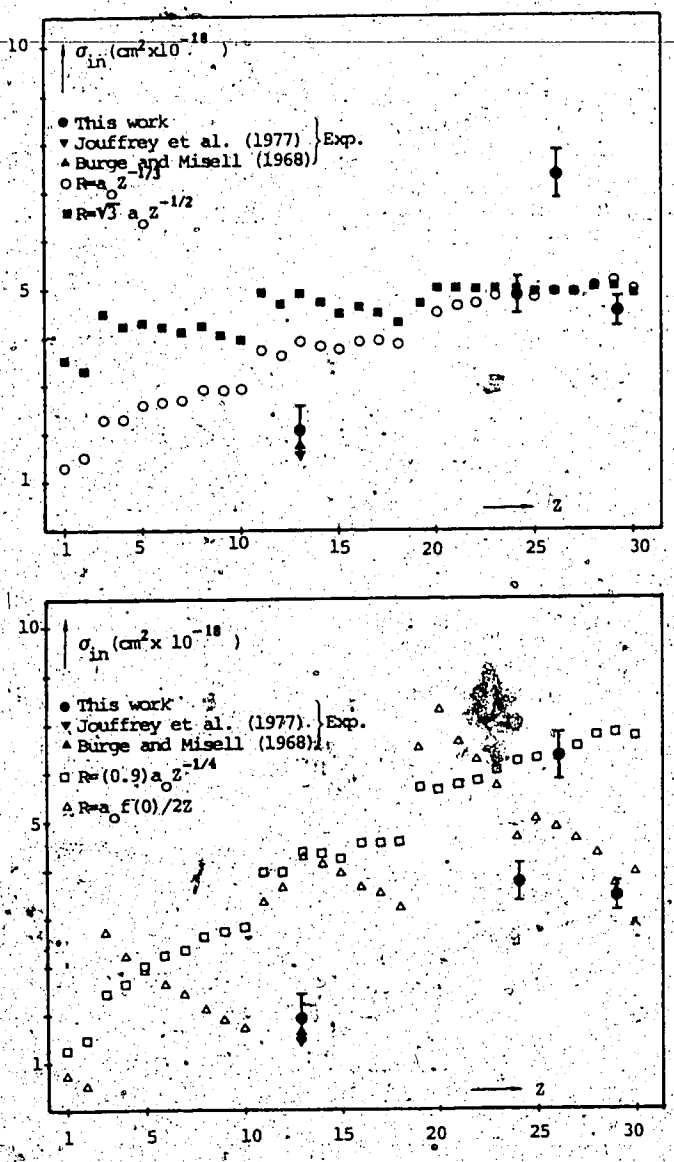

Figure 4.5 Total-inelastic cross-section as a function of the atomic number (Z) for 80keV electrons. σ_{in} was calculated using eq. (2.17) and the different expressions for R.

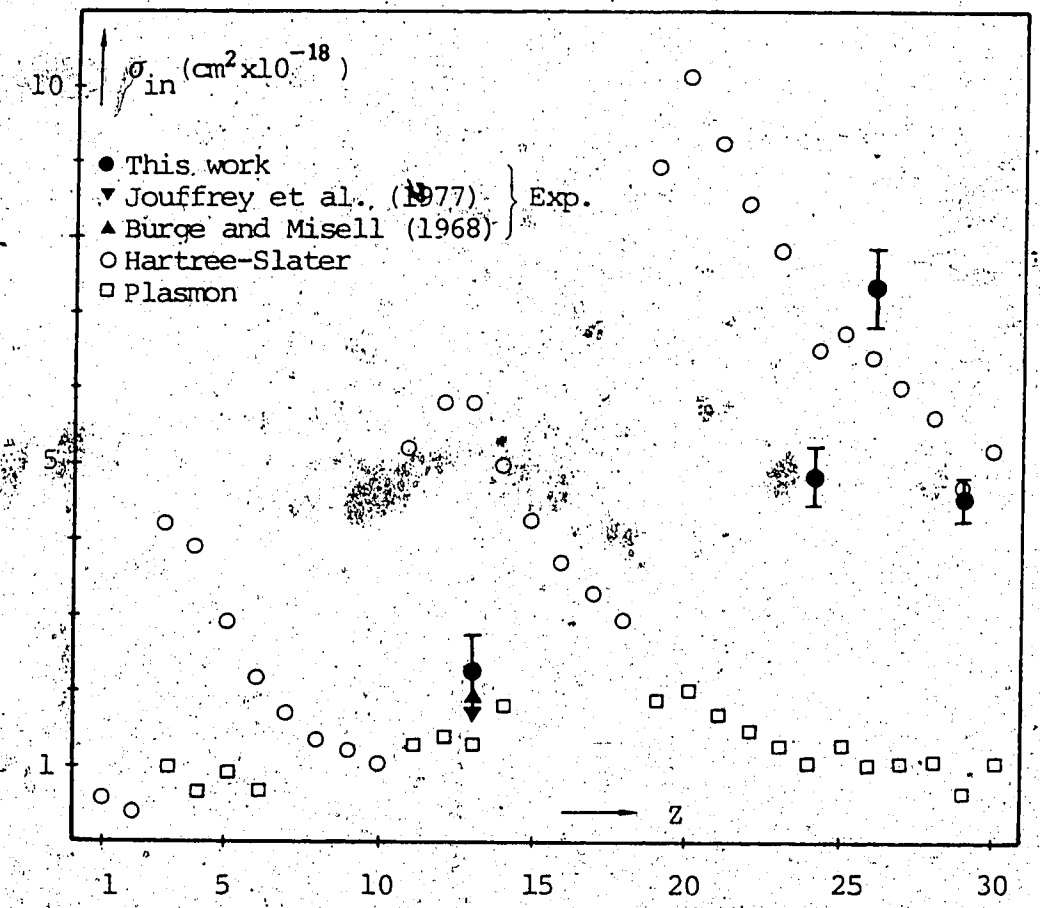

Figure 4.6 Inelastic cross-section as a function of the atomic number (Z) for 80keV electrons. The calculations are based on the Hartree-Slater and Plasmon model.

BIBLIOGRAPHY

Berger, M.J. and Seltzer, S.M. (1982) U.S. National Bureau of Standards Publication NBSIR 82-2550, Washington, D.C. 20234.

Bethe, H. (1930) Annal. Phys., 5, 325.

Bohm, D. and Pines, D. (1953) Phys. Rev., 92, 609.

Born, M. (1926) Z. Physik., 37, 863.

Burge, R.E. and Misell, D.L. (1968) Philos. Mag., 18, 216.

Colliex, C., Cosslett, V.E., Leapman, R.D., and Trebbia P. (1976) Ultramicroscopy, 1, 301.

Compton, A.H. (1930) Phys. Rev., 35, 928.

Dirac, P.A.M. (1930) Proc. Cambridge Phil. Soc., 26, 376.

Doyle, P.A. and Turner, P.S. (1968) Acta Cryst., A24, 390.

Egerton, R.F. (1978a) Ultramicroscopy, 3, 243.

Egerton, R.F. (1982) Microbeam Analysis, Ed. Heinrich K.F.J., p43.

Egerton, R.F. (1981) Proc. EMSA, p198.

Egerton, R.F. (1975) Philos. Mag., 31, 199.

Egerton, R.F. (1979a) Ultramicroscopy, 4, 169.

Egerton, R.F. (1979b) Ultramicroscopy, 4, 221.

Egerton, R.F. (1980) Proc. EMSA, p130.

Egerton, R.F. (1978b) Ultramicroscopy, 4, 39.

Fermi, E. (1928) Z. Physik., 48, 73.

Ferrel, R.A. (1956) Phys. Rev., 101, 554.

Fock, V. (1930) Z. Physik, 61, 126.

Haine, M.E. and Agar, A.W. (1959) Brit. J. Appl. Phys., 10, 341.

Hartree D.R. (1957) The calculation of atomic structures. John Wiley and Sons Inc., New York.

Hartree, D.R. (1928) Proc. Cambridge Phil. Soc., 24, 1928.

Hosoi, J., Oikawa, T., Inoue, M., Kokubo, Y., and Hama, K. (1981) Ultramicroscopy, 7, 147.

Inokuti, M., Saxon, R.P., and Dehmer, J.L. (1975) Int. J. Radiat. Phys. Chem., 7, 109.

Inokuti, M. (1971) Rev. Mod. Phys., 43, 297.

Inokuti, M., Dehmer, J.L., Bear, T., and Hanson, J.D. (1981) Phys. Rev. A, 23, 95.

Jouffrey, B., Kihn, Y., Perez, J.Ph., Sevely, J., and Zanchi, G. (1977) Fifth International Conference on High Voltage Electron Microscopy, Kyoto, Japan.

Joy, D.C., Egerton, R.F., and Maher, D.M. (1979) Scanning Electron Microscopy, Ed. OJohari (Chicago: SEM Inc.) 817.

Isaacson, M. and Johnson, D. (1975) Ultramicroscopy, 1, 33.

Langemore, J. Wall, J. and Isaacson, M. (1973) Optik, 38, 385.

Leapman, R.D., Rez, P., and Mayers, D.F. (1980) J. Chem.

Phys., 72, 1932.

Leisgang, S. (1952) Z. Physik, 132, 183.

Lenz, F. (1954) Z. Naturforsch., 9a, 185.

Manson, S.T. (1972) Phys. Rev., A6, 1013.

McGuire, E.J. (1971) Phys. Rev., A3, 267.

Morse, P.M. (1932) Phys., Z., 33, 443.

Powell, C.J. (1976) Rev. Mod. Phys., 48, 33.

Raman, C.U. (1928) Indian J. Phys., 3, 357.

Slater, J.C. (1930) Phys. Rev., 36, 57.

Slater, J.C. (1930) Phys. Rev., 35, 210.

Thomas, L.H. (1926) Proc. Cambridge Phil. Soc., 23, 542.

Turner, J.E. Roecklein, P.D. and Vora, R.B. (1970) Health Phys., 18, 159.

Weast, R.C. and Mevin, J.A. (1981) Handbook of Chemistry and Physics, pE68.

Wentzel, G. (1927) Z. Physik, **40**, 590.

Zaluzec, N.J. (1980) Proc. EMSA, p112.

Zener, C. (1930) Phys. Rev., **36**, 51.